THE ASTROPHYSICAL JOURNAL, 459:110–132, 1996 March 1

LINE STRENGTHS AND LINE STRENGTH GRADIENTS IN S0 GALAXIES

DAVID FISHER,[1,2] MARIJN FRANX,[1,3] AND GARTH ILLINGWORTH[2]

Received 1995 May 10; accepted 1995 September 5

ABSTRACT

Line strengths and their gradients in Mg, Fe, and Hβ have been determined for a sample of 20 S0 galaxies in order to study the stellar populations of their bulges and disks and to investigate their relationship to elliptical galaxies. Data are also presented for the elliptical galaxy NGC 1700 and the E/S0 NGC 3585. We find that S0 galaxies generally follow a similar, though possibly steeper, relationship between central Mg_2 line strength and central velocity dispersion as found for elliptical galaxies. The S0 galaxies show no dependence between Fe line strengths and central velocity dispersion—similar to the behavior observed in elliptical galaxies. The central Mg/Fe ratios in the luminous S0 galaxies show an overabundance of Mg to Fe with respect to solar element ratios. The disks (at 1 h) and bulges (at 1 r_e) show Mg/Fe ratios lower than those found in the central regions. The magnitudes of the Mg and Fe line-strength gradients within the galaxies are found to be correlated, i.e., objects with steep Mg gradients have correspondingly large Fe gradients.

We infer bulge and disk gradients for the nine most edge-on galaxies for which we have both major- and minor-axis profiles. The metal line strengths decrease with radius along the major and minor axes in the bulge-dominated central regions. At larger radii, however, the major-axis metal line strength profiles flatten while the minor-axis bulge profiles fall to lower values. Representative color maps in $B-R$ are presented that display a separation between bulge and disk colors corresponding to the metal line strength profiles. Based on our Mg_2 profiles, the average metal gradient found in the disks of our subsample is $\Delta[Fe/H]/\Delta(r/h) = -0.08 \pm 0.06$, which corresponds to a reduction in the mean metallicity of the disk stellar population by $\lesssim 15\%$ per disk scale length (h). These shallow metallicity gradients are approximately a factor of 2–3 smaller than those derived for the disks of late-type spiral galaxies from H II regions and are consistent with previous investigations that showed a trend for disk metallicity gradients to decrease toward earlier Hubble types. As inferred from our Mg and Fe line strengths, the mean size of the bulge metallicity gradients is $\Delta[Fe/H]/\Delta\log r = -0.7 \pm 0.4$, which is steeper than typical elliptical galaxy gradients.

Our findings do not support formation scenarios in which bulges formed either from heated disk material at late times after disk formation or through dissipationless stellar merging, as neither process includes mechanisms for producing the observed metallicity gradients. Our observations are better explained in terms of formation via dissipative collapse (or merging) at early times.

Subject headings: galaxies: abundances — galaxies: elliptical and lenticular, cD — galaxies: stellar content

1. INTRODUCTION

This paper is the first from a program to measure the chemical, kinematic, and structural properties of S0 galaxies. Here we study the stellar populations of 20 S0 and two elliptical galaxies by way of an analysis of their line strengths and gradients in Mg, Fe, and Hβ. The second part of our program will be an analysis of the stellar kinematics of this galaxy sample through absorption-line–derived rotation curves and velocity dispersion profiles. Additional spectra, to be presented in a forthcoming work, that enlarge the sample of objects and extend the observed wavelength region have been obtained. Multicolor broadband CCD imaging has been obtained for ~ 50 S0 galaxies and also will be presented in a future report.

The S0 galaxy class was initially postulated to be the transitional state between the most highly flattened ellipticals and the most early-type spirals (Hubble 1936, p. 36; Sandage 1961, p. 7). In this picture, S0 galaxies were characterized as being composed of a spheroidal bulge and a flattened disk with little gas, dust, or large-scale star formation. Additionally, the S0 galaxies were to have no spiral structure and to lie at the high bulge-to-disk ratio (B/D) end of the spiral sequence. It has generally been assumed that the bulges of S0 galaxies are kinematically hot with $r^{1/4}$-law light profles while the kinematically cooler rotating disks have exponential light profiles. A number of quantitative investigations (e.g., Kent 1985; Bothun & Gregg 1990) have had moderate success modeling the light distributions of S0 galaxies with a combination of de Vaucouleurs and exponential profiles, which lends support to the two-discrete-components picture.

A central question concerning the formation of S0 galaxies is whether they are primordial objects, having formed as S0, or are a result of evolutionary processes, i.e., once-normal spirals that were stripped of their gas (see Sandage & Visvanathan 1978; Dressler 1980; Larson, Tinsley, & Caldwell 1980). Concerning the former idea, Larson et al. (1980) suggested that the gas-poor nature of S0 galaxies could be the result of gas consumption by star formation since, in the absence of a gas-replenishment mechanism, this

[1] Kapteyn Astronomical Institute, University of Groningen, Postbus 800, 9700 AV Groningen, The Netherlands; fish, franx@astro.rug.nl.

[2] UCO/Lick Observatory, Board of Studies in Astronomy and Astrophysics, University of California, Santa Cruz, CA 95064; gdi@ucolick.org.

[3] Harvard-Smithsonian Center for Astrophysics, 60 Garden Street, Cambridge, MA 02138.

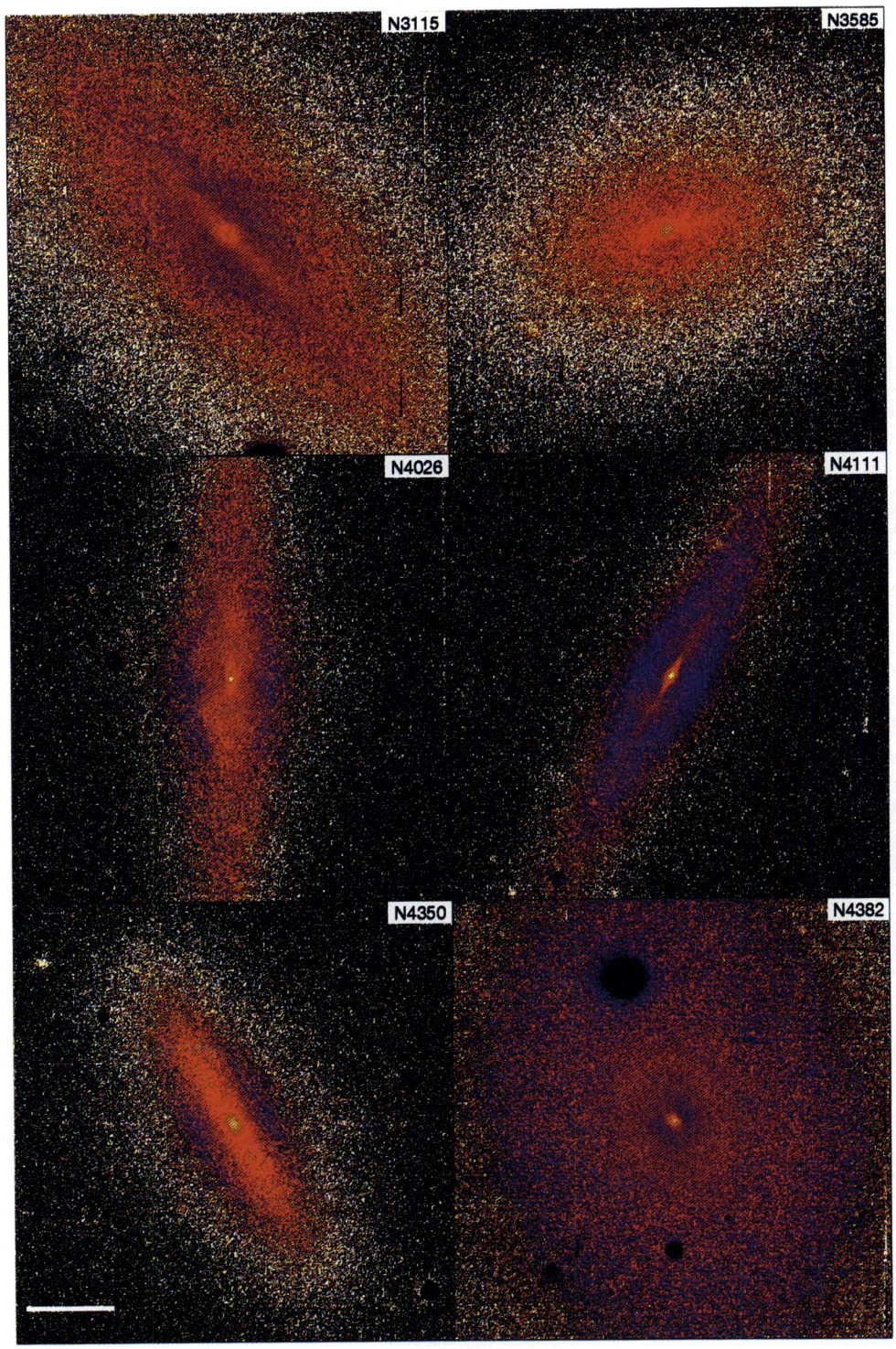

FIG. 5.—Mosaic of $B-R_C$ images for six of the galaxies in our sample. The color scale was chosen such that larger $B-R_C$ corresponds in the image to redder color and lower $B-R_C$ to bluer color. In all cases the nuclei show the reddest $B-R_C$ colors. For the four edge-on S0 galaxies (NGC 3115, NGC 4026, NGC 4111, NGC 4350), a distinction between the approximately constant-color disks and bluer outer bulges is apparent. A similar, though less pronounced, effect is observed in the disky E7/S0 galaxy NGC 3585. Note the blue ring surrounding the nucleus of the face-on S0 galaxy NGC 4382. The figure is oriented with north toward the top and east to the left. All images are the same size (148″ × 148″), and a 30″ long scale bar is shown. Bright stars have been masked.

FISHER, FRANX, & ILLINGWORTH (see 459, 110)

timescale is considerably shorter than a Hubble time. With respect to the latter possibility, Spitzer & Baade (1951) indicated that S0 galaxies in clusters could be formed from spirals whose disk gas was removed by galaxy-galaxy collisions. Ram-pressure stripping from the intergalactic medium (IGM) (Gunn & Gott 1972; Melnick & Sargent 1977), gas removal via galactic winds (Faber & Gallagher 1976), and gas evaporation from the hot IGM (Cowie & Songaila 1977) are some of the mechanisms suggested for the conversion from spiral to S0 galaxy.

Evidence exists to support the position that S0 galaxies owe at least some aspects of their formation to environmental effects. It has long been known that there are more early-type galaxies in denser environments (Hubble & Humason 1931; Morgan 1961; Abell 1965; Oemler 1974). It has also been observed that within a cluster the proportion of spirals increases with increasing distance from the cluster's center (Melnick & Sargent 1977). These results were confirmed by Dressler (1980), who used galaxy surface density as the independent parameter, indicating that local environmental properties play a role in galaxy morphology. However, Dressler offered three reasons why S0 galaxies could *not* be swept spirals: (1) there are numerous S0 galaxies in the field whose origin cannot be due to cluster-stripping processes; (2) the density–morphological type relation is the same in rich clusters (where stripping models would predict more S0 galaxies) as it is in poor, irregular ones; (3) the bulges of S0 galaxies are substantially more luminous than those of present-day spirals, and B/Ds of S0 galaxies are larger than those of spirals in all density regimes.

The sequence of bulge and disk formation in S0 galaxies is another open issue. Traditional formation models have disks forming later than bulges (Larson et al. 1980; Schechter 1990). The question is difficult to answer for S0 galaxies because the common tracers of star formation are largely absent. Some studies based on optical and IR photometry have concluded that the stars in S0 disks are younger than those in the bulges (Caldwell 1983; Gregg 1989b; Bothun & Gregg 1990). Recent simulations, however, show that it is possible for bulges to be made *after* the formation of a disk. Pfenniger (1993) has considered two scenarios in which bulges are formed later than disks: (1) small bulges made as a result of the formation and destruction of a bar and (2) large bulges resulting from the accretion of small satellites on an existing small bulge. Furthermore, Kormendy (1993) has presented observations used to argue that some galactic bulges, primarily those with box- or peanut-shaped isophotes, are composed of heated disk material.

Previous work on the stellar populations of S0 galaxies has mainly been limited to photometric investigations. The optical broadband study of Sandage & Visvanathan (1978) concluded that there is no evidence of young stellar populations in S0 galaxies. Burstein (1979a) obtained narrow-band photometry of four S0 disks and stated that they were the same age as the S0 nuclei and other ellipticals. In Caldwell's (1983) study of the nuclei and disks of 16 S0 galaxies, which used an Mg absorption index and broadband aperture photometry, the conclusion was reached that the disks of S0 galaxies are probably younger than the bulges, but the exact amounts were model dependent. Optical and IR aperture photometry was collected by Bothun & Gregg (1990) of the bulges and disks of 35 S0 galaxies. They decomposed the light profiles of their sample into $r^{1/4}$ bulges and exponential disks in order to derive "true" disk colors. A comparison with model $J-K$ and $B-H$ colors led Bothun & Gregg to conclude that the disks of their S0 galaxies were 3–5 Gyr younger than the bulges, a result they interpreted as being caused by a longer timescale for disk formation, rather than recent star formation.

The spectrophotometric study of Gregg (1989a, b) examined the nuclei and disks of a sample of 14 S0 galaxies and found evidence for hot subpopulations in the disks of roughly half his sample. With the assumption that the old populations of S0 disks are similar to those of ellipticals, Gregg (1989b) concluded that these hot subpopulations are young rather than metal-poor. These subpopulations were broken up by Gregg into those that are actively forming stars and those that have intermediate ages ($\sim$3–5 Gyr). Gregg indicated that his observations and modeling supported the view that S0 galaxies have evolved from spiral or spiral-like objects.

A drawback to investigating stellar populations photometrically is that narrow- and broadband data suffer from inherent limitations as population diagnostics. Specifically, broadband colors are incapable of accurately distinguishing the effects of age and metallicity on an integrated stellar population (Worthey 1994). The use of spectroscopic absorption-line strengths provides a solution to many of the problems encountered with photometry. Comprehensive stellar-population models have and are being generated by a number of groups, and these models are claimed to have the ability to distinguish between the effects of age and metallicity on observed line strengths (see, e.g., Worthey 1994; Weiss, Peletier, & Matteucci 1995, hereafter WPM). There has been little work on the line strengths of S0 galaxies, and the main goal of the present study is to use this important tool as a means of investigating the relative ages and metallicities of S0 galaxy bulges and disks. Through the comparison of S0 galaxy stellar populations to those in normal ellipticals, we aim to elucidate the general characteristics of the early-type galaxy family.

This paper is organized as follows: The sample of objects selected for study is described in § 2. The reduction and analysis procedures are discussed in § 3. The line strength results are given in § 4. A discussion of the implications of our findings is presented in § 5, and a summary and concluding remarks are given in § 6. Notes on the individual objects are given in Appendix A. Figures and tabulated line strength results for each galaxy are presented in Appendix B.

2. SAMPLE SELECTION

The galaxies chosen for this study are limited to Hubble morphological types S0, SB0, and SA0. As a group, these objects are referred to throughout this paper as S0 galaxies. Only if a certain morphological type is being discussed will the specific classification be used. The elliptical galaxy NGC 1700 and the E/S0 galaxy NGC 3585 are also included because they add to the comparison sample of Fisher, Franx, & Illingworth (1995a, hereafter FFI). They are also interesting in their own right (NGC 1700 has a counter-rotating stellar core [Franx, Illingworth, & Heckman 1989; González 1993], and NGC 3585 has an embedded disk component [Bender et al. 1993]).

The sample consists of objects in the field, small groups, and rich clusters. Galaxies at a variety of inclinations are present—from nearly face-on objects (e.g., NGC 4382 and

NGC 6703) to edge-on systems (e.g., NGC 4111 and NGC 4762). Deriving line strengths requires high signal-to-noise ratio (S/N) data, so we gave preference to the brightest objects available during the allocated observing periods. Although our sample is not complete in any sense, a criterion that nearly all the objects obey is that they are relatively nearby, with recession velocity $v_z \lesssim 2000$ km s^{-1} and total apparent B magnitude $B_T \lesssim 11.5$.

In Table 1 the Hubble types from both Sandage & Tammann (1981, RSA) and de Vaucouleurs et al. (1991, RC3) are given. The RSA catalog uses subscripts in order to distinguish between S0 galaxies with no trace of absorption lanes ($S0_1$) and later types with narrow absorption features ($S0_3$). The RC3 uses the notation $S0^-$ for early stages and $S0^+$ for late-stage S0 galaxies. There are clearly some discrepancies between the two classification sources. As an example, the RSA classifies NGC 4036 as a late-type $S0_3$/Sa while the RC3 gives this object an "earlier" $S0^-$ designation. Inspection of our B and R broadband CCD images clearly reveals dust in the bulge and inner disk of NGC 4036, which indicates that the RSA classification is more accurate in this case. The only other object in our sample that clearly shows the presence of an extended dust lane is NGC 5866.

Both NGC 4251 and NGC 4762 are galaxies classified as SB0 by the RC3, compared with unbarred classifications by the RSA. The galaxy NGC 4251 is nearly edge-on, and an ellipse-fitting algorithm applied to our R-band CCD images shows that while the position angle of NGC 4251 does not vary significantly with radius, the ellipticity profile is

TABLE 1

LOG OF OBSERVATIONS

Galaxy	RSA	RC3	T	Date	Exp	PA_{obs}	PA_{mj}
NGC 936	$SB0_{2/3}$/SBa	$SB0^+$	−1	20 Dec 1992	2400	45	135
NGC 1461	$S0_2$	SA0°	−2	20 Dec 1992	3000	158	155
...	...	...	...	20 Dec 1992	2791	68	...
NGC 1700	E3	E4	−5	18 Mar 1993	2400	65	65
NGC 2560	...	S0/a	.0	18 Mar 1993	2400	93	93
...	...	...	...	18 Mar 1993	2400	3	...
NGC 3115	$S0_1$	$S0^-$	−3	16 May 1993	2400	43	43
NGC 3384	$SB0_1$	$SB0^-$	−3	15 May 1993	2400	53	53
...	...	...	...	7 Mar 1992	2400	143	...
NGC 3412	$SB0_{1/2}$	SB0°	−2	17 May 1993	2700	155	155
...	...	...	...	17 May 1993	2400	65	...
NGC 3585	E7/$S0_1$	E7	−5	18 Mar 1993	2400	107	107
...	...	...	...	18 Mar 1993	2400	17	...
NGC 3607	$S0_3$	SA0°	−2	16 May 1993	2400	120	120
NGC 3941	$SB0_{1/2/a}$	SB0°	−2	17 May 1993	2400	10	10
...	...	...	...	17 May 1993	1387	100	...
NGC 3998	$S0_1$	SA0°	−2	15 May 1993	2400	140	140
NGC 4026	$S0_{1/2}$	S0	−2	25 Apr 1992	2400	178	178
...	...	...	...	25 Apr 1992	2400	88	...
NGC 4036	$S0_3$/Sa	$S0^-$	−3	16 May 1993	2400	85	85
...	...	...	...	17 May 1993	2400	175	...
NGC 4111	$S0_1$	$SA0^+$	−1	7 Mar 1992	2400	150	150
...	...	...	...	7 Mar 1992	2400	60	...
NGC 4251	$S0_1$	SB0	−2	16 May 1993	2400	100	100
...	...	...	...	17 May 1993	2400	190	...
NGC 4350	$S0_1$	SA0	−2	18 Mar 1993	2400	28	28
...	...	...	...	18 Mar 1993	2400	118	...
NGC 4382	$S0_1$	$SA0^+$	−1	18 Mar 1993	2400	179	179
...	...	...	...	18 Mar 1993	2400	89	...
NGC 4550	E7/$S0_1$	SB0°	−1.5	25 Apr 1992	2400	178	178
...	...	...	...	25 Apr 1992	2400	88	...
NGC 4754	$SB0_1$	$SB0^-$	−3	15 May 1993	2400	23	23
...	...	...	...	15 May 1993	2400	113	...
NGC 4762	$S0_1$	SB0°	−2	24 Apr 1992	3600	32	32
...	...	...	...	25 Apr 1992	2400	122	...
NGC 5866	$S0_3$	$SA0^+$	−1	16 May 1993	2400	128	128
...	...	...	...	24 Apr 1992	2400	34	...
...	...	...	...	24 Apr 1992	2400	[a]126	...
...	...	...	...	16 May 1993	2400	[b]38	...
NGC 6703	...	$SA0^-$	−2.5	17 May 1993	1071	60	60

NOTES.—Galaxy types taken from the RSA and from the RC3. T type and major-axis position angles, PA_{mj}, are taken from the RC3.

[a] Offset 6″ north, parallel to major axis.

[b] Offset 4.″5 northwest, parallel to minor axis.

complex—declining with radius, then rising, and then falling at our farthest measures. The major-axis surface brightness profile of NGC 4251 displays a number of dips and plateaus. These types of features have been mentioned as signatures of edge-on barred galaxies (Kormendy 1979). A visual inspection of our CCD images of NGC 4762 gives no impression that a bar is present in this edge-on system. The ellipse-fitting to NGC 4762 shows only the presence of a strong disk component on the basis of the cos 4θ term, and no distinguishing behavior in the position angle or ellipticity profiles is observed. Similarly to NGC 4251, however, the major-axis surface brightness profile of NGC 4762 is complex. On the basis of their images and modeling, Wakamatsu & Hamabe (1984) suggested that NGC 4762 could be described as containing four separate components: a nuclear bulge, bar, lens, and outer ring. Our kinematic profiles of NGC 4762 (to be presented in a future study) provide evidence that supports the existence of a bar. We summarize with the remark that the five galaxies NGC 936, NGC 3384, NGC 3412, NGC 3941, and NGC 4754 are clearly barred S0 galaxies while the cases for NGC 4251 and NGC 4762 are less secure.

3. DATA REDUCTION AND ANALYSIS

The data analyzed here were collected at Lick Observatory. The spectra were obtained with the 3 m Shane telescope and are the result of five observing runs (a total of eight usable nights). The red side of the KAST double spectrograph was employed for all runs. The detector was a thinned Reticon 400 × 1200 CCD with 27 μm pixels. The instrumental resolution was 3.1 Å (FWHM), which corresponds to an instrumental dispersion of $\sigma = 75$ km s^{-1}. The slit width was 2″, the slit length 145″, and the pixel scale 0.″8 pixel^{-1}. Details of dates, exposure times, and slit positions are given in Table 1. All data reductions were performed with the interactive image-reduction package VISTA (Lauer, Stover, & Terndrup 1983).

The spectra collected for the present study were obtained simultaneously with another program concerning brightest cluster galaxies (BCGs). The basic reduction procedures used to reduce the S0 data are identical to those described in our kinematic study of BCGs (Fisher, Illingworth, & Franx 1995b, hereafter FIF). The end product of these standard reduction techniques is a two-dimensional, geometrically rectified spectrum, binned logarithmically in the wavelength direction and linearly in the spatial direction. A sample spectrum is shown in Figure 1. Displayed is a deredshifted spectrum extracted from the central row of our major-axis frame of NGC 3384. The dominant contribution to the light in our S0 spectra comes from giant stars. The many features seen in the spectrum of NGC 3384 are real (S/N $\gtrsim$ 100).

Described below are specifics concerning the definition and measurement of absorption-feature indices and corrections to the Lick-IDS system. These procedures are similar to those used in our study of BCG line strengths (FFI), and we refer the interested reader to that paper for a more detailed description of measurement and correction techniques. In § 3.2 we discuss the disk and bulge fitting to our images.

3.1. *Line Strength Index Measurement*

Three wavelength regions are needed to define a spectral index: an interval covering the feature of interest and a pair of continuum bandpasses on each side of the feature. The strength of each spectral index is a measure of the flux in the central bandpass compared to a continuum level set by the sidebands. Indices are measured either as an equivalent width in angstroms (atomic indices) or as the ratio of line depth to continuum level in magnitudes (molecular indices).

The system of line strength indices used here is a result of a long-term project at Lick Observatory that employed the Shane telescope and image dissector scanner (IDS) (Faber et al. 1985; Burstein, Faber, & González 1986; Gorgas et al. 1993). The full set of 21 indices is presented in a recent paper from the Lick-IDS series (Worthey et al. 1994). The wavelength region covered by the observations obtained here contains the well-known magnesium triplet Mg b, Hβ, and a number of iron lines. In Figure 1 we show the regions covered by the line-strength indices and continuum bandpasses studied in the present work.

Two steps are required to convert our line-strength measurements to the Lick-IDS system: (1) a correction to account for the difference in spectral resolution between our data and the Lick-IDS data and (2) a correction for the galaxy's stellar velocity dispersion. Our resolution-correction technique consisted of broadening our spectra to the Lick-IDS resolution ($\sigma_{\rm IDS} = 200$ km s^{-1} at 5200 Å [González 1993]) with a Gaussian filter. This broadening was performed prior to measurement of the line indices. However, the kinematics of the objects were determined from a Fourier fitting program (described in FIF) before this broadening was applied.

A galaxy's stellar velocity dispersion weakens the strength of its absorption lines. In addition, since galaxies typically have a radial gradient in their velocity dispersion, the amount that the absorption features are diluted by velocity dispersion changes with radius. To make comparisons of measured galaxy line strength indices with stellar models, corrections must be made to convert observed galaxy line strengths to those they would have if measured in a single star (i.e., $\sigma = 0$ km s^{-1}). The only stellar observations we made were of G, K, and M giants as velocity templates for our kinematic analysis. These stars were used to derive empirical correction factors for each index to account for velocity dispersion. We artificially broaden our

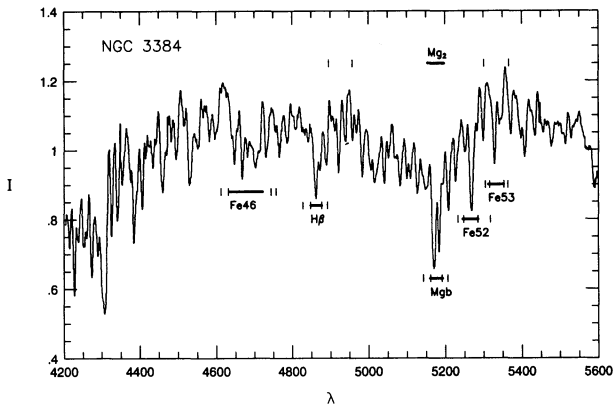

FIG. 1.—Deredshifted spectrum from the central row (0.″8 pixel^{-1}) of our major-axis exposure of NGC 3384. The data have a resolution of 3.1 Å (instrumental $\sigma \sim 75$ km s^{-1}). The stellar velocity dispersion of this spectrum is $\sim$140 km s^{-1}. The heavy horizontal lines delineate the region covered by the Lick-IDS line strength indices used here. The pairs of vertical lines on each side of the indices show the region covered by the associated continuum sidebands.

stellar observations with a series of Gaussian filters (from $\sigma = 0$ to $\sigma = 500$ km s^{-1} in 20 km s^{-1} increments). The full set of line strength indices is then measured in the stellar spectra over the range of broadenings. Polynomial fits for each index are then made, which results in multiplicative correction factors that need to be applied to our measured galaxy indices on the basis of their velocity dispersion profiles. As an example, for $\sigma_{gal} = 200$ km s^{-1} the correction for the Fe5335 index is $\sim 30\%$, less than 10% for the Mg b and Fe5270 indices, and nearly zero for the Hβ and Mg_2 indices.

Spectra were summed along the slit until a desired S/N was reached—typically S/N = 30–50 pixel^{-1}. The Fourier fitting routine fitted a broadened and redshifted stellar template to the binned galaxy spectra, and each binned row was deredshifted. For the galaxy sample the line strength profiles measured from the two sides of the nuclei were consistent to within our measured errors (see Tables 9 and 10). Therefore, we added the spectra from the two sides of the nucleus (after correcting for rotation) at corresponding radii and derived index measurements from these higher S/N, co-added spectra.

For the Mg_2 index, one further correction is needed. In the reduction of the Lick-IDS data a tungsten lamp was used as a relative calibrator of the instrumental spectral response, and thus the Lick-IDS data were not fluxed. Our data have been fluxed using spectrophotometric standards, and a correction is needed to place our Mg_2 measurements on the Lick-IDS system. González (1993) found that a constant offset of 0.017 mag needs to be added to the fluxed data in order to account for this difference in spectral shape. This correction has been applied to our Mg_2 measurements.

The sky level was determined from the outer parts of each galaxy frame. At each wavelength, a region ~ 30 pixels wide to either side of the galaxy nucleus was linearly interpolated and subtracted. While this method has the undesirable effect of subtracting the portion of the galaxy's spectrum present at the slit ends, it has the benefit of accurately removing the true sky level in addition to removing smooth patterns of scattered light. As a check on the amount of galaxy light that was subtracted from our spectra by use of this method, we calculated the galaxy flux at the last measured radial bin divided by the galaxy flux in the region where the sky level was determined. These ratios were determined from our broad R-band CCD images for a number of the objects in our sample. The galaxy for which this effect was the greatest was NGC 3115, in which this ratio along our major-axis spectrum was 2.0, i.e., 50% of the galaxy light in the last measured bin was subtracted by taking the sky level at the slit ends. The next most significant case was for the face-on galaxy NGC 4382, in which the flux ratio was 3.3 along the major axis. The edge-on galaxy NGC 4350, to which we devote considerable discussion, had a flux ratio of 4.8 along the major axis. At the other extreme, the major axis of NGC 2560, the faintest object in our sample, had a flux ratio $\gtrsim 20$. The minor-axis measurements, particularly for the edge-on objects, will be less affected by sky-subtraction errors. As an example, the last measured bin for the minor axis of NGC 4350 has a flux ratio of 22.

Half of our sample of objects show, at some level, emission from Hβ, [O III] 4959 Å, and/or [O III] 5007 Å (see Table 2). The index most affected by this is Hβ. In the most severe cases, the Hβ absorption feature can be entirely filled in and an emission line seen. We have made no attempt to correct for this effect theoretically, based on interstellar

TABLE 2

GALAXY PARAMETERS

Galaxy	B_T^0 (mag)	D (Mpc)	M_B (mag)	D/B	h	h (kpc)	ϵ_D	r_e	r_e (kpc)	ϵ_B	σ_0 (km s^{-1})	Emission? (Y/N)
NGC 936.....	10.98	21.7	−20.70	1.5	33″	3.5	0.23	11″	1.2	0.11	181	Y
NGC 1461.....	12.66	17.9	−18.60	1.3	22	1.9	0.73	5	0.4	0.19	197	N
NGC 1700.....	12.00	50.4	−21.51	0.2	4	1.0	0.09	37	9.0	0.30	217	N
NGC 2560.....	14.08	68.7	−20.11	0.6	17	5.7	0.84	3	1.0	0.17	201	N
NGC 3115.....	9.75	13.6	−20.92	0.3	36	2.4	0.87	29	1.9	0.31	239	N
NGC 3384.....	10.75	12.9	−19.80	0.9	55	3.4	0.52	10	0.6	0.16	138	N
NGC 3412.....	11.35	12.9	−19.20	1.1	25	1.6	0.42	8	0.5	0.22	103	N
NGC 3585.....	10.50	15.1	−20.40	<0.1	4	0.3	0.07	57	4.2	0.43	203	N
NGC 3607.....	10.87	22.7	−20.91	<0.1	4	0.4	0.41	50	5.5	0.12	215	Y
NGC 3941.....	11.27	15.8	−19.72	0.8	20	1.5	0.31	11	0.8	0.21	131	Y
NGC 3998.....	11.54	17.6	−19.69	0.4	36	3.1	0.27	11	0.9	0.15	297	Y
NGC 4026.....	11.60	17.6	−19.63	0.6	27	2.3	0.87	12	1.0	0.22	181	Y
NGC 4036.....	11.52	23.2	−20.31	0.9	24	2.7	0.76	15	1.7	0.13	166	Y
NGC 4111.....	11.62	17.6	−19.61	0.5	25	2.1	0.87	6	0.5	0.45	134	Y
NGC 4251.....	11.54	11.1	−18.69	0.3	17	0.9	0.77	20	1.1	0.29	118	N
NGC 4350.....	11.87	20.0	−19.64	0.7	15	1.5	0.81	12	1.2	0.26	186	Y
NGC 4382.....	9.95	20.0	−21.56	1.7	53	5.1	0.27	23	2.2	0.17	172	N
NGC 4550.....	12.40	20.0	−19.11	2.3	14	1.4	0.71	4	0.4	0.36	80	Y
NGC 4754.....	11.38	20.0	−20.13	0.7	49	4.8	0.50	13	1.3	0.15	171	N
NGC 4762.....	11.05	20.0	−20.46	1.4	44	4.3	0.92	13	1.3	0.19	129	Y
NGC 5866.....	10.87	13.0	−19.70	<1	28	1.8	0.73	37	2.3	0.11	139	Y
NGC 6703.....	11.97	24.3	−19.96	0.4	52	6.1	0.09	19	2.2	0.04	186	N

NOTES.—Total B-band "face-on" magnitudes, B_T^0, are corrected for Galactic and internal extinction, and for redshift from RC3. Distances (D) in Mpc calculated from mean group velocities using $H_0 = 75$ km s^{-1} Mpc^{-1}. Group velocities taken, in order of priority, from Nolthenius 1993, Garcia 1993, and Faber et al. 1989 (see Table 8). The distances for the galaxies NGC 2560 and NGC 3941, which are not found in the aforementioned group catalogs, are calculated with v_{3K} values taken from RC3. The B-band total absolute magnitudes, M_B, were determined from the given total apparent magnitudes, B_T^0, and distances, D. The following parameters were determined from the disk-bulge fitting routine as explained in § 3.2: disk-to-bulge ratio (D/B), disk scale length (h) in arcseconds and kiloparsecs, disk ellipticity (ϵ_D), bulge effective radius (r_e) in arcseconds and kiloparsecs, and bulge ellipticity (ϵ_B). The central stellar velocity dispersion (σ_0, in km s^{-1}) was calculated within a 4″ × 2″ aperture. The last column indicates whether emission features (Hβ, [O III] 4959 Å, and/or [O III] 5007 Å) are apparent in the spectra.

medium predictions, or from an empirical standpoint. Rather, we present the indices as measured and make note of the existence of any emission.

3.2. *Disk and Bulge Decomposition*

Broad *B*- and *R*-band images were obtained for all the objects in our sample with the Lick Observatory's 1 m Nickel telescope and a Loral 2048 × 2048 thick phosphor-coated CCD binned 2 × 2, yielding a scale of 0.″36 pixel^{-1}. From these images we have constructed color maps, ellipse fits, and extracted surface brightness profiles. The details of our image analyses will be presented in a future work.

The decomposition of spiral galaxies into disk and bulge components has been widely used as a tool for the study of galaxy structure (e.g., Kormendy 1977b; Burstein 1979b; Boroson 1981; Kent 1985). The most common method, and that utilized here, is to parameterize the disk and bulge components by empirical fitting functions. The de Vaucouleurs $r^{1/4}$ law is used for the bulge component and an exponential profile for the disk. The functions are fit to the observed major- and minor-axis surface brightness profiles by means of a least-squares routine with the characteristic brightnesses, scale lengths, inclinations, and ellipticities as free parameters. In Table 2 we list the exponential disk scale length (h) in arceseconds and kiloparsecs, disk ellipticity (ϵ_D), $r^{1/4}$ bulge effective radius (r_e) in arcseconds and kiloparsecs, and bulge ellipticity (ϵ_B). Also given in Table 2 is the disk-to-bulge ratio (D/B), corrected for the ellipticity of the bulge and disk components (i.e., corrected for the effect of inclination to the observed line of sight).

While the two-component model is a generally good description of the S0 galaxy light profiles, problems were often encountered with the barred objects (see § 2) and those with other higher order structures. Specifically, the major axes of NGC 4026, NGC 4111, NGC 4251, and NGC 4762 all showed the characteristic "stepped" brightness profile of a lens (see Kormendy 1977a). The prominent dust lane in NGC 5866, which obscures the central brightness peak of the bulge, prevented an accurate decomposition from being made for this SA0 galaxy.

As our derived line strengths are a measure of the integrated bulge-plus-disk starlight along a particular major- or minor-axis position angle, the images are needed in order to assign the line strengths to a bulge and/or disk component. We have selected a subsample of the nine most edge-on galaxies for which the bulge and disk components are most easily separable. For these objects, the minor-axis profiles are assumed to be representative of the bulge, and on the basis of the decomposition, we can determine at what radius the disk light dominates the major-axis profiles.

4. RESULTS

Appendix A provides notes on the individual objects. Plots of the derived Mg_2, Hβ, Fe5270, and Fe5335 line strength measurements for all the galaxies in our sample are presented in Appendix B (Fig. 10). The Fe4668 and Mg b indices were also measured but are not displayed because of space considerations. Because the strength of the Mg_2 feature, which is measured in magnitudes, typically allows it to be measured to a larger radius than the atomic indices, the radial intervals over which we measured the Mg_2 feature are different than for the other indices. In Appendix B we present the line strength measurements for the atomic indices (Table 9) and for the Mg_2 index (Table 10). *All line strengths presented in the tables and figures throughout this paper have been fully corrected to the Lick-IDS system, as described in § 3.*

TABLE 3

CENTRAL LINE STRENGTHS

Galaxy	Fe4668	Hβ	Mg b	Mg_2	Fe5270	Fe5335
NGC 936...	6.00	...	4.30	0.320	2.95	2.60
NGC 1461...	6.26	1.79	4.41	0.335	3.30	2.81
NGC 1700...	8.66	1.98	4.20	0.309	3.27	3.03
NGC 2560...	6.72	1.70	4.31	0.315	2.99	2.92
NGC 3115...	7.89	1.80	4.71	0.354	3.52	3.37
NGC 3384...	8.42	2.00	4.27	0.326	3.46	3.33
NGC 3412...	6.36	2.26	3.63	0.233	3.11	2.74
NGC 3585...	7.64	1.87	4.45	0.321	3.35	3.11
NGC 3607...	7.49	...	4.66	0.335	3.29	3.11
NGC 3941...	7.44	...	3.99	0.263	3.20	3.01
NGC 3998...	7.00	...	...	0.339	...	...
NGC 4026...	5.36	...	3.85	0.265	...	2.79
NGC 4036...	7.73	...	4.91	0.321	3.09	2.86
NGC 4111...	6.99	...	3.63	0.237	...	...
NGC 4251...	6.50	2.21	3.75	0.270	3.20	2.89
NGC 4350...	8.12	...	4.67	0.353	3.33	3.11
NGC 4382...	5.70	2.57	3.32	0.267	2.87	2.71
NGC 4550...	4.04	...	3.23	0.191	...	2.41
NGC 4754...	8.22	1.84	4.55	0.344	3.56	3.42
NGC 4762...	6.16	...	4.11	0.279	3.08	2.91
NGC 5866...	4.67	...	3.43	0.234	2.72	2.69
NGC 6703...	8.40	1.91	4.39	0.301	3.21	2.58

NOTES.—Line strengths as measured within the central 4″ of the 2″ wide slit. No Hβ values are given for objects in which the Hβ feature was contaminated by emission.

Table 3 lists the adopted central line strengths for each galaxy as determined for the central 4″ of the slit (i.e., for a 2″ × 4″ aperture). Galaxies for which the central Hβ feature was contaminated by emission do not have quoted $H\beta_0$ values. Bad columns coincident with an absorption feature occasionally prevented measurement of a particular index, with the result that some of the objects do not have measurements for all indices. Disk values for the nine galaxies in our edge-on sample are presented in Table 4. These disk values are taken from 5″–10″ long sections of the slit [i.e., 2″ × (5″–10″) apertures] centered at 1 disk scale length. Table 5 lists bulge line strengths at 1 r_e as inferred by the measured gradients. Objects whose disk or bulge Hβ features were affected by emission do not have quoted Hβ values.

Line strength gradient measurements for the S0 galaxies in our sample have not been made by other authors, and thus a direct comparison is not possible. Central Mg_2

TABLE 4

DISK LINE STRENGTHS

Galaxy	Fe4668	Hβ	Mg b	Mg_2	Fe5270	Fe5335
NGC 1461...	4.14	1.81	3.80	0.257	2.40	2.27
NGC 2560...	5.55	1.74	4.30	0.286	2.97	2.74
NGC 4026...	3.32	...	3.60	0.200	...	2.16
NGC 4036...	6.41	...	3.97	0.261	3.31	2.77
NGC 4111...	3.42	...	2.90	0.186	...	...
NGC 4251...	4.60	2.26	3.47	0.215	3.01	2.64
NGC 4350...	5.53	1.64	4.16	0.280	2.94	2.59
NGC 4550...	3.32	...	3.08	0.169	...	2.33
NGC 4762...	...	...	...	0.236	3.07	2.85

NOTES.—Line strengths as measured within 5″–10″ long sections of the 2″ wide slit at a distance of 1 scale length. No Hβ values are given for objects in which the Hβ feature was contaminated by emission.

TABLE 5

BULGE LINE STRENGTHS

Galaxy	Hβ	Mg b	Mg_2	Fe5270	Fe5335
NGC 1461.....	1.65	4.22	0.265	2.51	2.61
NGC 2560.....	1.72	3.99	0.277	2.75	2.64
NGC 4026.....	...	3.37	0.159	...	2.57
NGC 4036.....	...	3.38	0.193	2.78	2.53
NGC 4111.....	...	3.22	0.218	...	...
NGC 4251.....	2.03	3.28	0.185	2.64	2.44
NGC 4350.....	1.64	3.06	0.172	2.21	2.20
NGC 4550.....	...	2.90	0.164	...	...
NGC 4762.....	...	...	0.194	2.28	...

NOTES.—Bulge line strengths were determined from the least-square fits to the minor-axis gradients (see Table 6) at a distance of 1 effective radius. For NGC 4251 and NGC 4762, in which our minor-axis measurements do not extend to 1 r_e, we quote the last measured values from our profiles. No Hβ values are given for objects in which the Hβ feature was contaminated by emission.

results collected from a variety of sources are presented in Bender, Burstein, & Faber (1993, hereafter BBF) for the centers of 19 S0 galaxies, six of which are also in our sample. A comparison between our central values and those in BBF shows a mean difference of 0.020 mag in Mg_2. The typical errors in our central Mg_2 measurements are of order 0.01 mag and, for BBF, 0.01–0.02 mag. The BBF data for the six objects in common with our study come from three different sources, one of which is unpublished (the one containing four of the objects). We have reproduced similarly sized central measures as in BBF and used the same distance-aperture corrections (those given in Davies et al. 1987). However, the intrinsic line strength gradients in the objects, and differences in the seeing, resolution, and slit width, will influence the derived central values.

In our paper on BCG line strengths (FFI), comparisons were made between ellipticals that we measured using an identical setup as used here and results from other authors. In that study we found that the average differences (after all corrections to the Lick-IDS system) between our measurements and those of others were (in terms of us vs. them) $\langle H\beta \rangle = +0.091 \pm 0.163$, $\langle Mg\ b \rangle = -0.172 \pm 0.243$, $\langle Mg_2 \rangle = +0.004 \pm 0.012$, and $\langle Fe5270 \rangle = +0.114 \pm 0.272$. For some galaxies the differences between the various studies are significant, although the overall agreement is consistent with the quoted errors.

4.1. Mg *and* Fe *Line Strengths versus Velocity Dispersion*

The relationship between central Mg strength and central stellar velocity dispersion for early-type galaxies is a well-studied line strength correlation (see, e.g., Faber 1973; Terlevich et al. 1981; Dressler 1984; Dressler et al. 1987; BBF). The BBF study claimed that a single mean relation between the central Mg_2 index and σ_0 held for their entire sample of objects (cE, dE, luminous E, and S0 bulges) over 4 orders of magnitude in mass and surface brightness. A common explanation for the Mg_2-σ_0 relation has been that in kinematically hot, dissipative systems, the amount and rate of enriched gas inflow from evolved stars, and the ability to retain these metals, is an increasing function of the galaxy mass/potential (e.g., Larson 1975). A luminosity-metallicity relationship also exists for spiral galaxies over a similarly large range in galaxy size and abundance (Garnett & Shields 1987). Zaritsky, Kennicutt, & Huchra (1994, hereafter ZKH) found that the correlation between spiral and irregular galaxy luminosity and metallicity holds over a range of 10 mag in M_B and a factor of 100 in mean abundance.

The relation between central magnesium strength, Mg_2, and central velocity dispersion, σ_0, is shown in the top panel of Figure 2 for our sample of S0 galaxies. Also shown are measurements from Davies et al. (1987) for a subset of the Seven Samurai elliptical galaxies. Only a subset was used because we are concerned about the use of correction formulae (to account for the distance–aperture size effect) in scaling the observed Mg_2 and σ_0 values to the distance of Coma (as done in BBF). Our concerns are based on our observations that S0 galaxies can have different line-strength gradient sizes than elliptical galaxies (see § 4.3), making the correction factors inapplicable to both types of systems. Therefore, we have selected from Davies et al. only those elliptical galaxies found within a factor of 2 in distance from the Virgo Cluster, which is the typical range spanned by our data. These elliptical data, shown in Figure 2, come from the raw measurements of the Davies et al. (1987) sample.

The slope of the relation found by BBF for their entire sample of objects was $\Delta Mg_2/\Delta \log \sigma_0 = 0.20$, in agreement with what we find for the Davies et al. subsample of ellipticals, i.e., $\Delta Mg_2/\Delta \log \sigma_0 = 0.20 \pm 0.02$. A least-squares fit to our S0 data gives $\Delta Mg_2/\Delta \log \sigma_0 = 0.29 \pm 0.05$. This is marginally steeper than the elliptical relation. The suggestion from our data that there is a difference in relations between the elliptical and S0 galaxies depends heavily on the two low-σ_0 objects (NGC 3412 and NGC 4550). More measurements of low velocity dispersion S0 bulges ($\sigma_0 \lesssim 100$ km s^{-1}) are needed to check the validity of a possibly steeper S0 relation. We note that ZKH reported a luminosity-metallicity relation for spiral and irregular galaxies that was also steeper than the elliptical relation and suggested that, with time, the S + Irr relation might evolve toward the elliptical slope as irregulars fade and [O/H] increases. However, the fact that the S0 data generally fall within the region spanned by the elliptical galaxies indicates that S0 bulges share with elliptical galaxies some basic similarities in their star-formation histories.

The scatter about our relation is 0.022 mag in Mg_2 while the errors in Mg_2 are of order 0.01 mag. The BBF relation for their total sample of objects had a similar scatter in Mg_2 over the entire range of their relation. It is interesting that our S0 galaxy relation is similar in tightness to that of the BBF relation, considering the potential additional influence of a disk contribution to our central measurements. This scatter about the Mg_2-σ_0 relation is real and likely reflects a complexity of formation processes as well as age and metallicity variations. BBF estimated that the scatter about the mean relation implies a combined age and metallicity variation of $\sim 15\%$ for the luminous objects.

Residuals between the measured central Mg_2 values and those predicted by the fitted relation based on the measured central velocity dispersions were calculated. A search for correlations between the residuals and other galaxy kinematic, line strength, and structural parameters was made. The only correlation that was found was a weak trend for objects with signs of recent star formation (emission lines, blue nuclei, large Hβ) to have central Mg_2 values lower than that predicted by the Mg_2-σ_0 relation for their velocity dispersion. Similar behavior was noted by BBF in the context of ellipticals with high-frequency structure, as param-

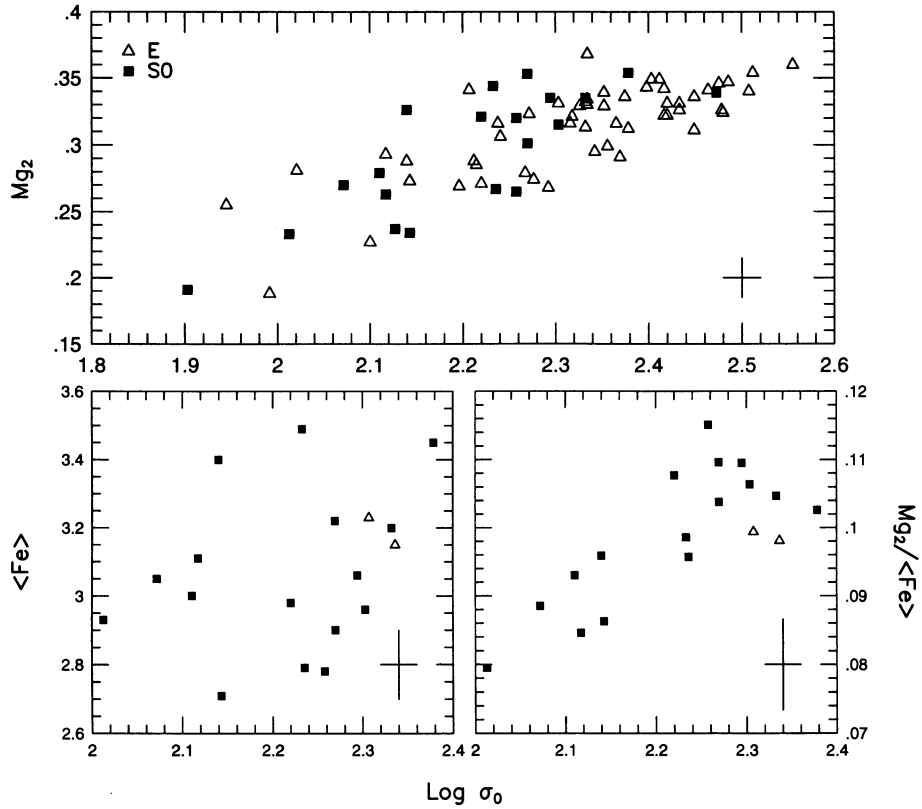

FIG. 2.—Mg and Fe line strengths vs. central velocity dispersion. All indices have been transformed to the Lick-IDS system. *Top*: Central Mg_2 index plotted against the logarithm of the central velocity dispersion (σ_0). The S0 galaxies from the present study (*squares*) and elliptical data from Davies et al. (1987) (*triangles*) are plotted. A typical set of error bars is shown. *Bottom left*: Central iron strength, $\langle Fe \rangle$ = (Fe5270 + Fe5335)/2, vs. velocity dispersion. In contrast to the Mg_2-σ_0 relation, the Fe line strengths show no dependence with velocity dispersion. *Bottom right*: Ratio of central magnesium index to central iron index, $Mg_2/\langle Fe \rangle$, plotted against velocity dispersion. An increase of Mg/Fe line strength ratio with velocity dispersion is seen.

eterized by the Schweizer et al. (1990) Σ-parameter, and those with kinematically distinct cores.

As an example, the galaxy NGC 4382, which displays strong central Hβ in absorption (Hβ_0 = 2.6 Å) and a blue nucleus, has a central Mg_2 that falls 0.035 mag below our fitted S0 relation. The continuum from the young component of stars in the center of NGC 4382 is likely diluting the light from the underlying old population, resulting in the low Mg_2 measurement. We note that NGC 1700, an elliptical with a counterrotating stellar core, lies very close to the elliptical Mg_2-σ_0 relation.

Five of the six "barred" galaxies in our sample (see § 2) show central Mg_2 strengths larger than predicted by the S0 Mg_2-σ_0 relation for their central velocity dispersion. Further observations of barred systems are needed to check the validity of this result and to investigate any connections between the line strengths and the presence of a bar.

The lower left panel of Figure 2 is a plot of central Fe line strength, defined as $\langle Fe \rangle$ = (Fe5270 + Fe5335)/2, versus velocity dispersion. In contrast to the Mg_2-σ_0 relation, the Fe line strengths display no correlation with velocity dispersion. A similar result for elliptical galaxies was demonstrated by González (1993). It is notable that S0 bulges share the behavior of elliptical galaxies by having no strong dependence between Fe abundance and object mass.

4.2. Mg/Fe *Ratio*

The lack of a correlation between Fe abundance and velocity dispersion for elliptical galaxies, in contrast to the behavior of Mg, results in an observed "overabundance" of Mg with respect to Fe in more massive systems. Using a set of α-enhanced stellar models, WPM reported that luminous elliptical galaxy observations could be reproduced with an Fe abundance that generally does not exceed the solar value. Because of the enhancement of α-peak elements, the total metal content in these models is, however, supersolar. The result is that giant elliptical galaxies have a ratio of Mg to Fe that is 0.3–0.7 dex above the solar value (WPM). This behavior is reproduced by our S0 nuclei, as shown in the lower right panel of Figure 2, using the ratio of the central Mg_2 index to the central iron measure, $\langle Fe \rangle$. The qualitative trend of increasing Mg/Fe ratio with velocity dispersion is seen in both the nuclei of S0 and elliptical galaxies.

In Figure 3 we show the Mg versus Fe relation for the nuclei, bulges, and disks of our S0 galaxies. Overlain on Figure 3 is the model grid of Worthey (1994) and a number of model tracks from WPM. The Worthey models assume solar abundance ratios while the WPM models are calculated with a variety of chemical compositions, including α-enhanced abundance ratios. The overall shallow slope of the Mg-Fe relation for the S0 galaxy nuclei is similar to that seen in ellipticals and BCGs (see, e.g., Worthey, Faber, & González 1992, hereafter WFG; Davies, Sadler, & Peletier 1993; Sil'chenko 1993; Carollo & Danziger 1994a; FFI) and indicates that the majority of the systems have central Mg/Fe ratios larger than solar. In the more luminous S0 nuclei the level of Mg enhancement can be large, comparable to that seen in elliptical galaxies (i.e., [Mg/Fe] ~ 0.3–0.5 dex). This behavior has been reported by Fisher (1994b) and similarly by Bender & Paquet (1995) for their samples of

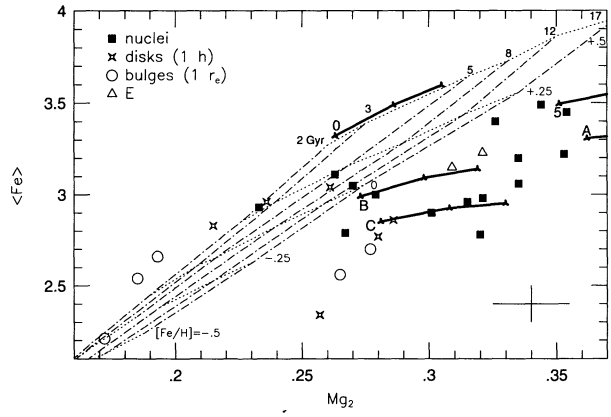

FIG. 3.—Mg/Fe ratio. Squares denote the central 2″ × 4″ values for the S0 nuclei (Table 3). Overlaid is the grid of Worthey (1994) for single-burst, coeval models with solar abundance ratios. Lines of constant age (*dot-dashed lines*) are given for 2, 3, 5, 8, 12, and 17 Gyr. Lines of constant metallicity (*dotted lines*) are shown for [Fe/H] = −0.5, −0.25, 0, +0.25, and +0.5. The majority of S0 nuclei display Mg/Fe ratios greater than scaled solar ratios and require α-enhanced models in order to be fit. From the subsample of edge-on objects, we show the 1 scale length disk (*stars*) and 1 effective radius bulge (*circles*) values (see Tables 4 and 5). The 1 *h* disk and 1 r_e bulge values are found with Mg/Fe ratios lower than their associated nuclear values. Central values for NGC 1700 and NGC 3585 are also given (*triangles*). Model tracks (*heavy lines*) from Weiss et al. (1995) are also shown for various stellar compositions from their α-enhanced models at 12, 15, and 18 Gyr. Stellar mixtures 0 ([Mg/Fe] = 0), B ([Mg/Fe] = 0.45), and C ([Mg/Fe] = 0.67) have $Z = 0.02$ and $Y = 0.28$. Mixture 5 ([Mg/Fe] = 0.45) and mixture A ([Mg/Fe] = 0.62) have $Z = 0.04$ and $Y = 0.32$.

objects. These large Mg/Fe ratios cannot be explained by simple scalings of solar abundances or realistic changes to the model ages (WFG; WPM). Both quicker star formation and flatter IMFs in the higher σ_0, more massive, systems have been offered as possible mechanisms for generating larger than solar Mg/Fe ratios (e.g., WFG). Sil'chenko (1993) obtained data for a sample of disk galaxies of types S0–Sc and concluded that the nuclear Mg/Fe ratios for these systems are consistent with solar values.

From our subsample of nine edge-on S0 galaxies, 1 effective radius bulge Mg_2 and $\langle Fe \rangle$ values have been measured for five of the systems (see Table 5) and 1 scale length disk values have been measured for six of the objects (see Table 4). From Figure 3, two of the bulges (NGC 1461 and NGC 2560) have Mg/Fe ratios larger than predicted by the Worthey models, and the remaining three (NGC 4036, NGC 4251, NGC 4350) have ratios either lower than or consistent with the model tracks. Three of the six disks have Mg/Fe ratios greater than solar (NGC 1461, NGC 2560, NGC 4350) while the other three (NGC 4036, NGC 4251, NGC 4762) are consistent with the Worthey-model predictions.

Inspection of Figure 3 shows that there is a range in the behavior of the slopes from the nuclei to the bulges and disks in the Mg-Fe plane. In relation to each other, the 1 effective radius bulge Mg/Fe ratios are typically lower than those found in the disks at 1 scale length. Compared to the central values, the general statement can be made that the 1 effective radius bulge and 1 scale length disk Mg/Fe line strength ratios are both lower than that found in their associated galaxy centers. The one exception among the six objects is for NGC 1461, in which the central and disk Mg/Fe ratios are similar. Bender & Paquet (1995) reported that in their sample of S0 galaxies, the disk Mg/Fe ratios were mostly consistent with solar element ratios. Concerning the bulges, our finding that the Mg/Fe ratio decreases with radius in the bulges contrasts with what has been observed in ellipticals and BCGs, where rough agreement is seen between the internal Mg/Fe profiles and constant Mg/Fe model predictions (e.g., WFG; FFI).

4.3. *Metal Line Strength Gradients*

A general feature of all the objects of our sample is that the maximum Mg_2 strength is always found at the object centers. In agreement with the standard picture (see § 1), our bulge/disk decompositions indicate that the central regions are dominated by light from $r^{1/4}$-law bulge components, and our entire sample displays similar major- and minor-axis metal line strength profiles in these innermost bulge regions ($r \ll 1\ r_e$). It is only for the galaxies in our edge-on subsample that differences between the major- and minor-axis metal line strength profiles are apparent.

The major- and minor-axis Mg_2 profiles for the nine galaxies in the edge-on subsample are shown in Figure 4. A common feature of the profiles in Figure 4 is that the major-axis Mg_2 gradients become shallow as the bulge light contribution decreases and the disk begins to dominate. Our measurements reach to a radius of at least 1 disk scale length of all nine of the objects in the subsample. Overall, the observations suggest that to 1 scale length the disk Mg_2 strength is roughly constant. There are, however, indications of structure in some of the galaxy profiles. This is most easily seen in the higher S/N observations of NGC 4036 and NGC 4350, where it appears that the disk Mg_2 strengths begin to slightly rise with radius beginning at the point where the bulge profile drops below that of the disk and continuing to ~1–2 scale lengths. The major-axis Mg_2 profile of NGC 4350 at radii beyond ~30″, i.e., 2 *h*, begins to drop sharply. This is the most convincing case in our subsample of declining Mg_2 strength in an S0 disk with radius.

The minor-axis behavior of the edge-on S0 galaxies is markedly different than that found along the major axis. In nearly every case, the minor-axis Mg_2 strength decreases to values lower than that found along the disk. The minor-axis gradients in the edge-on subsample display a uniform decrease in strength with radius that is qualitatively similar to the behavior observed in elliptical galaxies (see, e.g., Gorgas, Efstathiou, & Aragón-Salamanca 1990; Carollo & Danziger 1994a, b; Davies et al. 1993; González 1993; FFI). In NGC 4026, the region from 2″ to 6″ along the minor axis displays constant Mg_2 strength, but at larger radii the Mg_2 values decline.

It is important to determine whether the differences in Figure 4 between the major- and minor-axis Mg_2 profiles reflect real differences in the chemical composition of the galaxies (i.e., as a function of galactocentric radius) or are an effect of orientation. Therefore, we have scaled the major- and minor-axis profiles in Figure 4 on the basis of ellipticity profiles measured from our *R*-band images using standard isophote-fitting software. No scaling was done for radii $r < 2''$. These scaled Mg_2 profiles are plotted in Figure 4 along with the original measurements. For the galaxies NGC 1461, NGC 4111, and NGC 4550 the scaled major- and minor-axis profiles are similar and indicate that the contours of constant Mg_2 strength follow the galaxy *R*-band isophotes. In the remaining objects the distinction

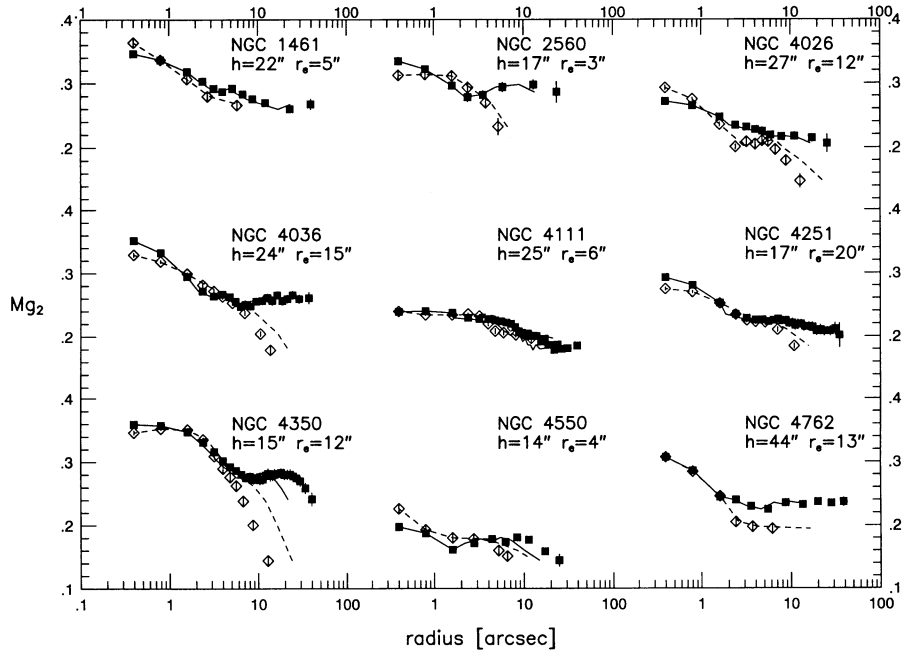

FIG. 4.—Major-axis (*squares*) and minor-axis (*diamonds*) Mg_2 profiles for the nine S0 galaxies in the edge-on subsample. The exponential disk scale length (h) and $r^{1/4}$-law bulge effective radius (r_e), as determined from our photometric decomposition, are given. Although the major- and minor-axis gradients in the bulge-dominated inner regions are similar, at larger radii the disk profiles flatten while the bulge Mg_2 strengths continue declining to lower values. This effect is still present in most cases even after the major-axis (*solid lines*) and minor-axis (*dashed lines*) measurements have been scaled for ellipticity.

between a disk with roughly constant Mg_2 strength and a bulge with decreasing Mg_2 strength persists despite the ellipticity scaling and demonstrates that the radial Mg abundance distribution in these objects is different in their disk and bulge components.

These differences in the major- and minor-axis metal line-strength profiles are often striking, and it is interesting to investigate whether similar behavior would be observed in broadband colors. In Figure 5 (Plate 1) we show $B-R_C$ color maps for a subset of our galaxy sample. Four nearly edge-on galaxies are given (NGC 3115, NGC 4026, NGC 4111, NGC 4350), the disky elliptical galaxy NGC 3585, and the face-on S0 NGC 4382. For the galaxies NGC 3115, NGC 3585, and NGC 4350, three separate components can be identified: a red nuclear region, a fairly constant color "disk" structure, and a bluer region above and below the disk. The outer bulge region of NGC 4026 also shows a blueing trend, but the presence of a thin, disklike structure is not readily apparent. In NGC 4111 a concentrated, thin, disky feature with $B-R_C \gtrsim 1.6$ mag is visible in the nuclear regions ($r \lesssim 4''$), surrounded by a bulge with $B-R_C \lesssim 1.5$ mag. The nucleus of NGC 4382 is quite red, $B-R_C \approx 1.7$, and is surrounded by a blue region ($B-R_C \approx 1.45$ mag) that almost forms a complete ring around the nucleus. Beyond this blue region, the $B-R_C$ profile of NGC 4382 becomes *redder* with increasing radius until, at radii $r > 20''$, the more conventional blueward trend is seen.

Of course, the presence of dust is a serious concern in the interpretation of these colors, and seeing effects can also act to increase the measured colors in the innermost regions. Michard & Marchal (1994) studied five of these galaxies (all except NGC 3585) and concluded that dust was likely to be present in NGC 4026 (they suggested it might be a "hidden Sa") and also in NGC 4111. Only upper limits on 100 μm flux have been measured for NGC 3115, NGC 3585, and NGC 4382 (Roberts et al. 1991), indicating that large amounts of dust are not present. Roberts et al. presented no dust measurements for NGC 4111. The estimated cool-dust masses (inferred from the 100 μm observations) are $2.3 \times 10^5\ M_\odot$ for NGC 4026 and $1.7 \times 10^5\ M_\odot$ for NGC 4350 (Roberts et al. 1991). We note that an inspection of our B and R broadband frames and the residual maps from the isophote-fitting for these six objects gives no indication of the presence of dust.

We can perform a test for the presence of dust in these galaxies by comparing the measured Mg_2 line strengths to the measured $B-R_C$ colors and model predictions. The Mg_2 line strengths should be relatively immune to the presence of the small amounts of dust being considered here—in contrast to the dust-sensitive $B-R_C$ colors. Color profiles were measured with 6 pixel–wide (2".16) cuts along the same position angles as the spectra. From these profiles, $B-R_C$ values were extracted at radii equivalent to those of our Mg_2 measurements. A plot of Mg_2 versus $B-R_C$ is given in Figure 6 with the Worthey (1994) model grid overlain. Figure 6 immediately shows that throughout NGC 4026 and in the central regions of NGC 4111 the $B-R_C$ colors are redder (by more than 0.1 mag) than predicted by their corresponding Mg_2 values and fall completely off the model locus. A few points in the very central regions of NGC 4350 and NGC 4382 also show $B-R_C$ colors redder than predicted by the Mg_2 values, but the level is not great (less than 0.1 mag), and seeing effects in these innermost regions could be largely responsible. The enhancement of Mg_2 in some of the galaxies with respect to the solar-neighborhood calibrating stars (see § 4.2) is noticeable as a trend for the Mg_2 measurements to appear too large for their associated $B-R_C$ colors when compared to the models. From these analyses we conclude that for the six galaxies shown in Figure 5 only NGC 4026 and the nuclear regions of NGC 4111 are likely to contain amounts of dust significant enough to affect their measured colors. For the remaining objects the $B-R_C$ colors and Mg_2 values are consistent with the model predictions, and the clear separations

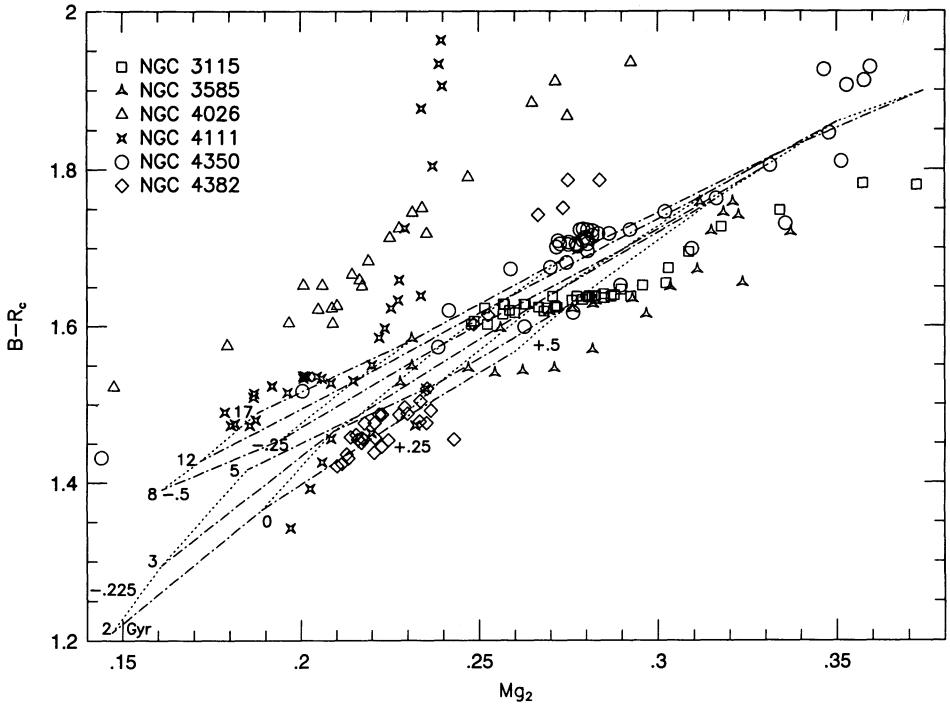

FIG. 6.—Color vs. Mg_2 for the objects displayed in Fig. 5. $B-R_C$ colors were measured at radii corresponding to our major- and minor-axis Mg_2 values. The entire profiles along both axes for each galaxy are shown. Overlaid is the model grid of Worthey (1994). The presence of dust throughout NGC 4026 and in the central regions of NGC 4111 is indicated by their high $B-R_C$ values compared to the model predictions on the basis of the measured Mg_2 strengths. The enhancement of Mg_2 with respect to the solar-neighborhood calibrating stars used in the models is also apparent.

between disk and bulge Mg_2 profiles (Fig. 4) are reflected in the color maps.

To investigate the behavior of the S0 bulge metallicity gradients and compare them to elliptical galaxy values we have made least-square fits to the minor-axis profiles. The mean gradient for all nine objects is $\Delta Mg_2/\Delta\log r = -0.10 \pm 0.06$. Excluding the extremely steep gradient seen in NGC 4350 ($\Delta Mg_2/\Delta\log r = -0.24 \pm 0.01$), the mean gradient for the remaining eight objects is $\Delta Mg_2/\Delta\log r = -0.09 \pm 0.03$. These S0 bulge gradients are marginally steeper than those typically found in elliptical galaxies, which have gradient magnitudes $\Delta Mg_2/\Delta\log r \approx -0.06$ (taking the mean from the results of Couture & Hardy 1988, Gorgas et al. 1990, Davidge 1992, and Davies et al. 1993). Using the Worthey (1994) models our S0 bulge Mg_2 gradients correspond to a metallicity gradient of Δ[Fe/H]/$\Delta\log r = -(0.53\text{–}0.59) \pm 0.35$. We note that this conversion to an [Fe/H] gradient is done under the assumption of constant age (15 Gyr). In § 4.4 we will show that a strict interpretation of the Worthey (1994) models indicates that age gradients are present, and a conversion to a metallicity gradient with this condition will be made.

There have been suggestions that the magnitudes of elliptical galaxy line strength gradients are correlated with various photometric and kinematic properties. Carollo, Danziger, & Buson (1993) reported a trend in their data for elliptical galaxies less massive than $10^{11}\ M_\odot$ to have increasing Mg_2 gradient sizes with increasing galaxy mass—a correlation in the sense predicted by dissipational formation models (Larson 1975; Carlberg 1984). However, González (1993) observed that gradient magnitudes *decreased* with increasing velocity dispersion in his sample of ellipticals, and FFI found no correlations between line strength gradients and either kinematic or photometric properties of the objects in their sample. We checked for correlations between the magnitudes of our bulge Mg_2 gradients and central velocity dispersion, central Mg_2 strength, and absolute bulge magnitude. Weak trends were seen for the gradient magnitudes to increase with velocity dispersion and central Mg_2 strength, but more data are needed to confirm this behavior.

A correlation is seen between the Mg and Fe gradient sizes themselves. In Figure 7 we show both major- and minor-axis Mg_2, Fe5270, and Fe5335 gradient magnitudes plotted against each other. These gradients, given in Table 6, are global logarithmic gradients (i.e., calculated for the full radial range of our measurements along each axis). The mean errors on the global gradient sizes are $\epsilon(\Delta Mg_2/\Delta\log r) = \pm 0.015$, $\epsilon(\Delta\log \text{Fe52}/\Delta\log r) = \pm 0.022$, and $\epsilon(\Delta\text{Fe53}/\Delta\log r) = 0.026$. The Mg and Fe indices are clearly linked, similar to the behavior seen in color gradients (see, e.g., Peletier et al. 1990; Balcells & Peletier 1994) and are noteworthy given the differing mechanisms by which Mg and Fe are produced. Therefore, although the net level of Fe in a galaxy is decoupled from the net Mg level (Fig. 2), their radial distributions are similar (particularly at radii beyond the nuclear regions).

Disk Mg_2 gradients were calculated for the nine objects in the edge-on subsample. These gradients are given in Table 7 as a function of scale length, absolute physical size (kpc), and logarithmically. Gradients were calculated as a function of different normalizing radii so comparisons could be made with spirals, which are generally measured versus either physical size or scale length, and with ellipticals, normally measured logarithmically. Inspection of Table 7 shows that these various normalizations give consistent results between the objects, i.e., disks with large gradients in one characterization are correspondingly steep relative to the other galaxies in another. The mean disk gradient for the subsample is $\Delta Mg_2/\Delta(r/h) = -0.01 \pm 0.02$, correspond-

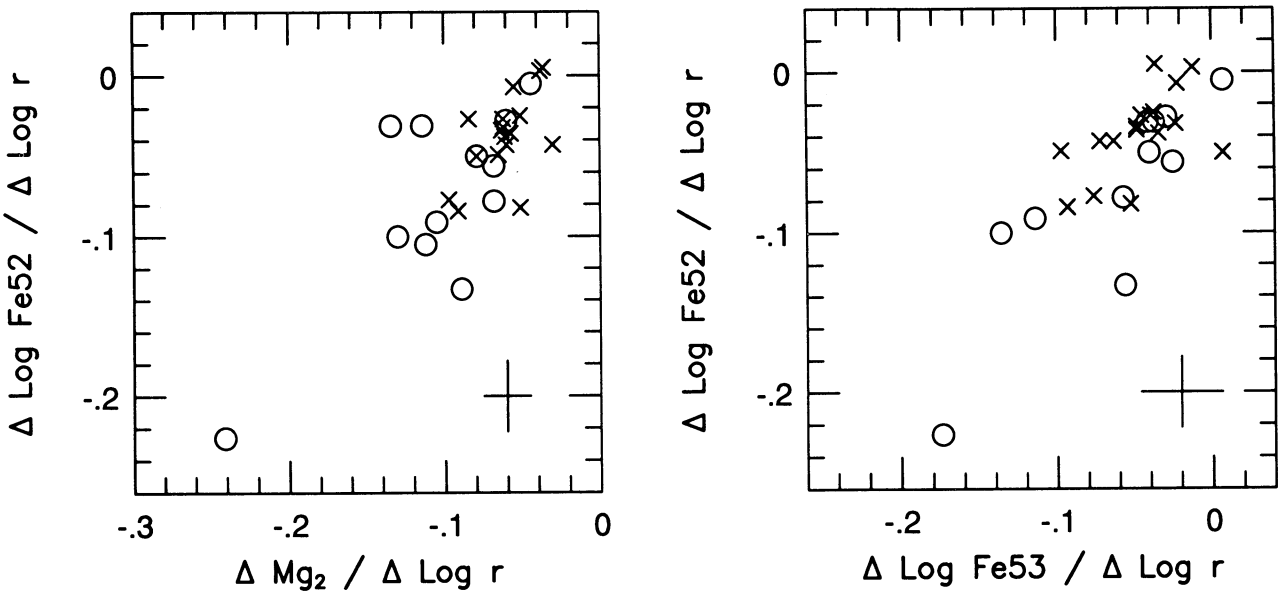

FIG. 7.—Mg and Fe line strength gradient correlations. Data from both the major (*crosses*) and minor (*circles*) axes are shown. Measurements refer to the global line strength gradients (see Table 6). The magnitudes of the Mg and Fe line strength gradients are correlated with one another. The data point with the steepest gradients is from the minor-axis measurement of NGC 4350.

ing to a metallicity gradient of Δ[Fe/H]/$\Delta(r/h) = -0.06 \pm 0.08$ on the basis of the Worthey (1994) calibration. Measured as a function of absolute physical size, our mean disk gradients are Δ[Fe/H]/$\Delta(r$ kpc$^{-1}) = -0.041 \pm 0.022$. These disk gradients are very shallow, corresponding to a reduction in the mean metallicity of the stellar population of approximately 10%–15% over 1 disk scale length, or less than 10% kpc^{-1}. Shallow gradients in S0 disks have also been reported by Fisher (1994b), Bender & Paquet (1995), and Fisher, Illingworth, & Franx (1995c).

The study of abundance gradients in spiral galaxies has focused primarily on measuring the ([O III] + [O II])/Hβ emission-line ratio in H II regions (e.g., Vila-Costas & Edmunds 1992; Zaritsky, Elston, & Hill 1990; ZKH). From these studies, typical spiral-disk (O/H) gradients of -0.18 dex h^{-1}, or -0.07 dex kpc^{-1}, have been reported. These gradients are based on spirals with a wide range in Hubble types, from Sa to Irr, though the mean galaxy type is typically Sc. Investigations of abundance gradients in Sa and Sb spiral disks have found abundance gradients shallower than those in the Sc galaxies (e.g., Oey & Kennicutt 1993). Complicating a direct comparison between our S0 metallicity gradients and those in spirals is that our line strengths are

TABLE 6

GLOBAL LINE STRENGTH GRADIENTS

	∇Fe4668		∇Hβ		∇Mg *b*		∇Mg_2		∇Fe5270		∇Fe5335	
GALAXY	Major	Minor	Major	Minor	Major	Minor	Major	Minor	Major	Minor	Major	Minor
NGC 936.....	...	−0.095	...	...	...	−0.041	...	−0.060	...	−0.028	...	−0.029
NGC 1461.....	−0.129	...	−0.009	−0.013	−0.030	−0.032	−0.051	−0.089	−0.082	−0.133	−0.052	−0.056
NGC 1700.....	−0.146	...	0.005	...	−0.064	...	−0.084	...	−0.027	...	−0.045	...
NGC 2560.....	−0.065	−0.088	−0.010	0.016	−0.001	−0.049	−0.030	−0.134	−0.043	−0.031	−0.063	−0.041
NGC 3115.....	−0.091	...	0.032	...	−0.042	...	−0.062	...	−0.027	...	−0.039	...
NGC 3384.....	−0.217	−0.171	−0.032	−0.009	−0.078	−0.061	−0.097	−0.068	−0.077	...	−0.076	...
NGC 3412.....	−0.133	−0.179	−0.034	−0.053	−0.044	−0.056	−0.061	−0.068	−0.038	−0.056	−0.034	−0.025
NGC 3585.....	−0.084	−0.260	0.009	0.000	−0.049	−0.122	−0.062	−0.130	−0.032	−0.100	−0.023	−0.136
NGC 3607.....	−0.093	...	...	...	−0.065	...	−0.063	...	−0.034	...	−0.048	...
NGC 3941.....	−0.105	−0.167	...	...	−0.037	−0.068	−0.057	−0.079	−0.036	−0.050	−0.048	−0.040
NGC 3998.....	−0.120	...	...	...	−0.109	...	−0.065	...	−0.049	...	−0.097	...
NGC 4026.....	−0.106	−0.284	...	...	−0.024	−0.053	−0.041	−0.092	...	...	−0.032	−0.039
NGC 4036.....	−0.076	−0.160	...	...	−0.083	−0.135	−0.055	−0.114	−0.007	−0.031	−0.022	−0.037
NGC 4111.....	−0.171	−0.280	...	...	−0.081	−0.063	−0.035	−0.021	...	...	...	...
NGC 4251.....	−0.097	−0.164	−0.004	−0.029	−0.020	−0.059	−0.051	−0.068	−0.025	−0.078	−0.037	−0.057
NGC 4350.....	−0.137	−0.396	0.006	−0.005	−0.043	−0.253	−0.060	−0.241	−0.043	−0.226	−0.072	−0.174
NGC 4382.....	−0.082	−0.083	−0.042	−0.039	0.018	−0.004	−0.036	−0.044	0.005	−0.005	−0.036	0.007
NGC 4550.....	−0.074	−0.266	...	...	−0.016	−0.083	−0.014	−0.052	...	...	−0.003	...
NGC 4754.....	−0.221	−0.209	0.005	−0.012	−0.078	−0.085	−0.091	−0.105	−0.084	−0.091	−0.093	−0.114
NGC 4762.....	−0.163	−0.159	0.018	...	...	−0.086	−0.038	−0.112	0.003	−0.105	−0.012	...
NGC 6703.....	−0.108	...	−0.038	...	−0.080	...	−0.079	...	−0.050	...	0.007	...

NOTES.—Logarithmic line strength gradients. For the atomic indices the gradients are measured as $\Delta\log(\text{index})/\Delta\log r$. For Mg_2 we calculate $\Delta Mg_2/\Delta\log r$. Gradients are for all measured values and extend to the limit of our data. For cases in which the seeing was affecting the indices in the inner regions, the gradients are for radii, $r \gtrsim 2''$. No Hβ values are given for objects in which the Hβ feature was contaminated by emission.

TABLE 7

DISK Mg_2 GRADIENTS

Galaxy	$\Delta Mg_2/\Delta(r/h)$	$\Delta Mg_2/\Delta(r\ \mathrm{kpc}^{-1})$	$\Delta Mg_2/\Delta \log r$
NGC 1461.....	-0.022 ± 0.004	-0.011 ± 0.002	-0.040 ± 0.007
NGC 2560.....	$+0.010 \pm 0.013$	$+0.002 \pm 0.002$	$+0.018 \pm 0.015$
NGC 4026.....	-0.013 ± 0.014	-0.005 ± 0.006	-0.012 ± 0.014
NGC 4036.....	-0.002 ± 0.011	-0.001 ± 0.004	-0.005 ± 0.026
NGC 4111.....	-0.040 ± 0.003	-0.019 ± 0.001	-0.062 ± 0.004
NGC 4251.....	-0.002 ± 0.017	-0.002 ± 0.018	-0.007 ± 0.061
NGC 4350.....	-0.016 ± 0.004	-0.011 ± 0.003	-0.047 ± 0.014
NGC 4550.....	-0.022 ± 0.006	-0.016 ± 0.004	-0.033 ± 0.010
NGC 4762.....	$+0.005 \pm 0.015$	$+0.001 \pm 0.003$	-0.008 ± 0.018

NOTES.—Disk gradients are determined along the major axes for radii, $r > 1\ r_e$, and extend to the limit of our measurements.

measuring the mean abundances in old stellar populations versus the present-day gas-phase metallicities that the spiral H II region measurements determine. This makes the comparison between mean abundances in S0 and spiral galaxies subject to evolutionary processes that could likely be different between these two types of systems. However, the *gradients* might presumably be less affected, and given that both Mg and O are α-peak elements that owe their formation to similar processes, a comparison could still be appropriate. A comparison between the S0 disk metallicity gradients measured here and those found in the spiral disks shows that S0 disks have metallicity gradients a factor of 2–3 times smaller than those seen in late-type spiral galaxy disks. The abundance gradients in the Sa- and Sb-type spirals have magnitudes roughly intermediate between the S0 and Sc galaxies. Our shallow S0 disk gradients are apparently independent of which normalizing radius we use. These results suggest that Hubble type is a significant parameter in the sizes of disk-galaxy abundance gradients.

4.4. *Metallicities and Ages*

Studies of spiral disks have found strong correlations between disk abundance and disk circular velocity (e.g., ZKH). In Figure 8 we plot the relation between 1 scale length disk Mg_2 strength and disk circular velocity for the nine S0 disks in our edge-on subsample. The disk v_{circ} determinations have been made on the basis of our kinematic and photometric profiles with the assumption that the subsample galaxies are edge-on. Corrections for integration through the line of sight and asymmetric drift were applied. A least-squares fit to the data gives the relation shown as a solid line: $Mg_2 = (0.46 \pm 0.10) \log v_{circ} - 0.87$. Although there is scatter (at $\sigma \sim 0.02$ mag) in the relationship, a clear trend is apparent for S0 disk metallicities to increase with v_{circ} and, hence, galaxy mass. Since there is little variation in Hubble type (see Table 1) for these galaxies, the link between disk abundance and global properties (i.e., mass) is strong. This is supported by the trend for disk Mg_2 strength to increase with both σ_0 and central Mg_2 strength (not shown). Followup studies for these objects are in progress and will address whether the disk metallicities show a dependence on either local kinematic or photometric structure.

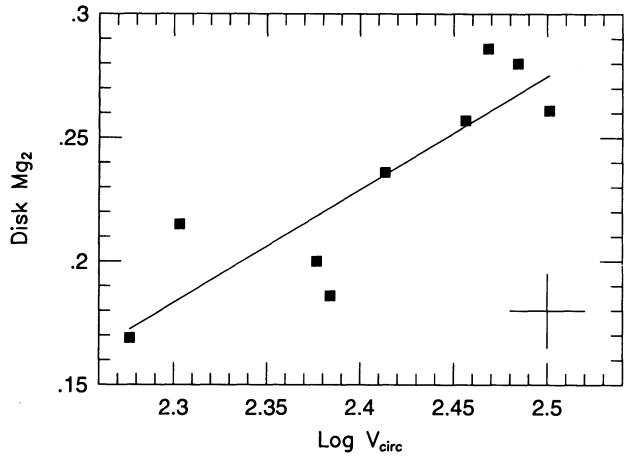

FIG. 8.—Disk (1 h) Mg_2 strength vs. disk circular velocity. Corrections to v_{circ} have been made to account for integration through the disk line of sight and asymmetric drift. The data suggest a relation between the stellar population of the disk and the circular velocity. A least-squares fit to the data, shown as a solid line, gives $Mg_2 = (0.46 \pm 0.10) \log v_{circ} - 0.87$.

The motivation for using line strengths as a means of studying stellar populations is the fact that broadband colors (and many indices) are incapable of distinguishing between the effects of age and metallicity on integrated galaxy light. Worthey (1994) has identified a number of indices that are claimed to break this degeneracy by being primarily sensitive to either age or metallicity and relatively immune to the other effect. One of the best age-sensitive indicators found by Worthey is the Hβ feature. Figure 9*a* plots the central Hβ strengths versus velocity dispersion for the S0 galaxies from the present study and elliptical and BCGs from the FFI and González (1993). A least-squares fit to the data (not shown) results in the relation $H\beta = -1.25 \pm 0.15 \log \sigma_0 + 4.62$ (excluding the data for NGC 4382). This relation is interesting. Initially, the trend might be attributed to the fact that among early-type galaxies higher σ_0 objects are generally redder and, therefore, would be assumed to have lower Hβ strengths, as our figure shows. However, the relationship between color and Hβ strength is not direct. Although star-forming galaxies will typically display blue colors and strong Hβ lines as expected, normal quiescent elliptical and S0 galaxies have color gradients but not Hβ gradients (Davidge 1992; González 1993; Davies et al. 1993; FFI).

If the Hβ index can be interpreted as an age indicator (i.e., Worthey 1994), then the relations seen in Figures 9*a* and 9*b* suggest that more massive early-type galaxies (those with larger σ_0 and higher Mg/Fe ratios) have experienced a longer period of time since their last burst of star formation (lower Hβ) than less massive galaxies. Alternatively, if the Hβ index is due to blue horizontal-branch stars, then the observed trends point toward initial mass function (IMF) variations between the galaxies as a possible source of the correlations. This would operate in the sense that the more massive galaxies have flatter IMFs than less massive galaxies. Flatter IMFs cause the helium–to–heavy-element ratio to decline as the proportion of massive stars is increased (Maeder 1992). The horizontal branch becomes redder as $\Delta Y/\Delta Z$ declines (Renzini 1993), resulting in lower Hβ strengths. As mentioned in § 4.2, flatter IMFs can also account for the increasing Mg/Fe in the more massive galaxies. We remark that these are just a sample of possible scenarios, but they demonstrate that the Hβ trends do not necessitate age variations between the galaxies if the source of the Hβ feature is not dominated by light from main-sequence turnoff stars.

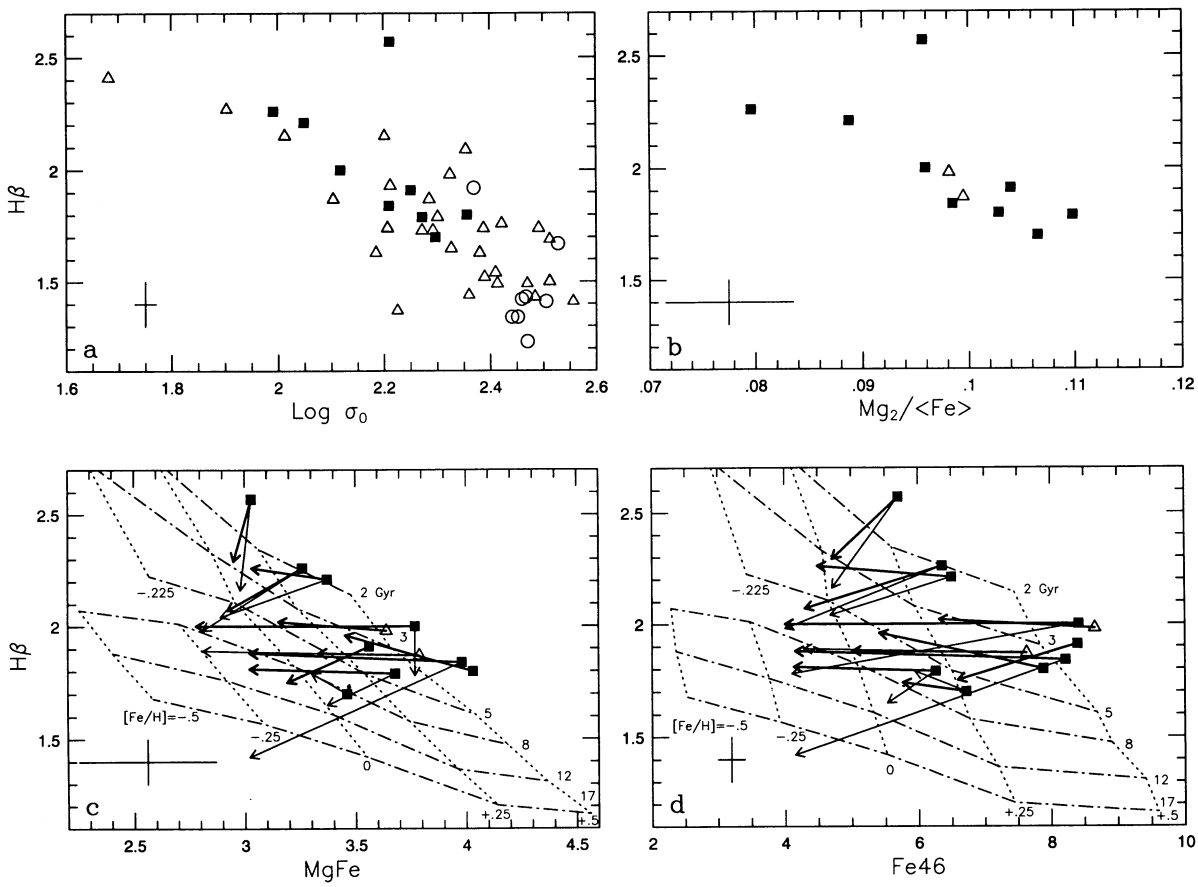

FIG. 9.—Correlations with Hβ. Only objects in which the Hβ feature was not contaminated by emission are displayed. (*a*) Central Hβ line strength plotted against central velocity dispersion. Squares denote the S0 galaxies from the present study, circles represent BCGs from FFI, and triangles are elliptical galaxies from FFI and González (1993). A trend is apparent toward higher σ_0 galaxies having lower Hβ strengths. The data at Hβ = 2.57 Å represent the nucleus of NGC 4382. (*b*) Central Hβ line strength vs. Mg/Fe ratio for our S0 galaxies (*squares*) and the two ellipticals in our sample (*triangles*). (*c*) Hβ line strength vs. the mean magnesium and iron strength MgFe = $(\mathrm{Mg}\ b \times \langle \mathrm{Fe} \rangle)^{1/2}$. Symbols denote the central measurements, and arrows extend to the last measured values along the major (*heavy solid lines*) and minor (*light solid lines*) axes. Overlaid is the Worthey (1994) model grid. (*d*) Hβ line strength vs. Fe4668 line strength. Symbols are as in (*c*).

Although there are exceptions (to be discussed below), for the majority of the S0 galaxies in which emission is not contaminating the Hβ feature, the Hβ gradients are quite shallow throughout the bulges and disks (see Table 6, Fig. 10). This result is similar to the behavior of the Hβ index in elliptical galaxies (Davidge 1992; González 1993; Davies et al. 1993; FFI). Exceptions to the flat Hβ profiles have been observed in elliptical galaxies with kinematically distinct cores (e.g., NGC 4073 in FFI). The flat Hβ gradients in the S0 galaxies are in marked contrast to the sizable metal line strength gradients. Figures 9*c* and 9*d* are plots of metal line strength versus Hβ. In Figure 9*c* we show MgFe = $(\mathrm{Mg}\ b \times \langle \mathrm{Fe} \rangle)^{1/2}$ versus Hβ, and in Figure 9*d* we give the Fe4668 index versus Hβ. The Fe4668 index is claimed to be the most metallicity-sensitive index in the Lick-IDS library and contains contributions from C_2 and Mg I 4703 Å (Worthey 1994).

In the presence of a falling abundance gradient, a constant-age population will display a *rising* Hβ profile with radius (under the Worthey assumptions about the origin of the Hβ feature). A simple explanation for this effect is that the Hβ index as measured in a metal-rich region has the light in the continuum bandpasses depressed by the strong metal lines, which gives rise to a lower Hβ index value than would be measured in a weaker lined region. Therefore, a strict interpretation of Figures 9*c* and 9*d* indicates that the flat gradients observed in Hβ are more consistent with a younger central population compared to the outer parts. These results suggest that the centers of the S0 galaxies are dominated by the light of a population having an age that is generally younger than their outer bulge ($r \gtrsim 1\ r_e$) and disk ($r \gtrsim 1\ h$) regions.

We find that some S0 galaxies display line strengths comparable to those found in normal bright ellipticals while others are much more weakly lined. On the basis of the Worthey models, the range of Hβ values shown in Figures 9*c* and 9*d* for our S0 galaxies indicates that they span a range in the time since their last burst of star formation from those with recent active star formation (e.g., NGC 4382 and NGC 5866) to those that have been dormant for long periods ($\gtrsim$10 Gyr). This spread in the time since the last star-formation episode as suggested by the models for the S0 galaxies is similar to that claimed for normal ellipticals under the same assumptions concerning the Hβ index (González 1993; FFI; Faber et al. 1995). None of the S0 galaxies, however, are as strong-lined as the strongest lined ellipticals, and none have central Hβ line strengths as low as those found in the largest elliptical galaxies (Fig. 9*a*). This suggests that while nearby elliptical and S0 galaxies exist over a range of ages (since their last burst of star formation) and metallicities, the elliptical galaxies extend further into the older age, higher metallicity region.

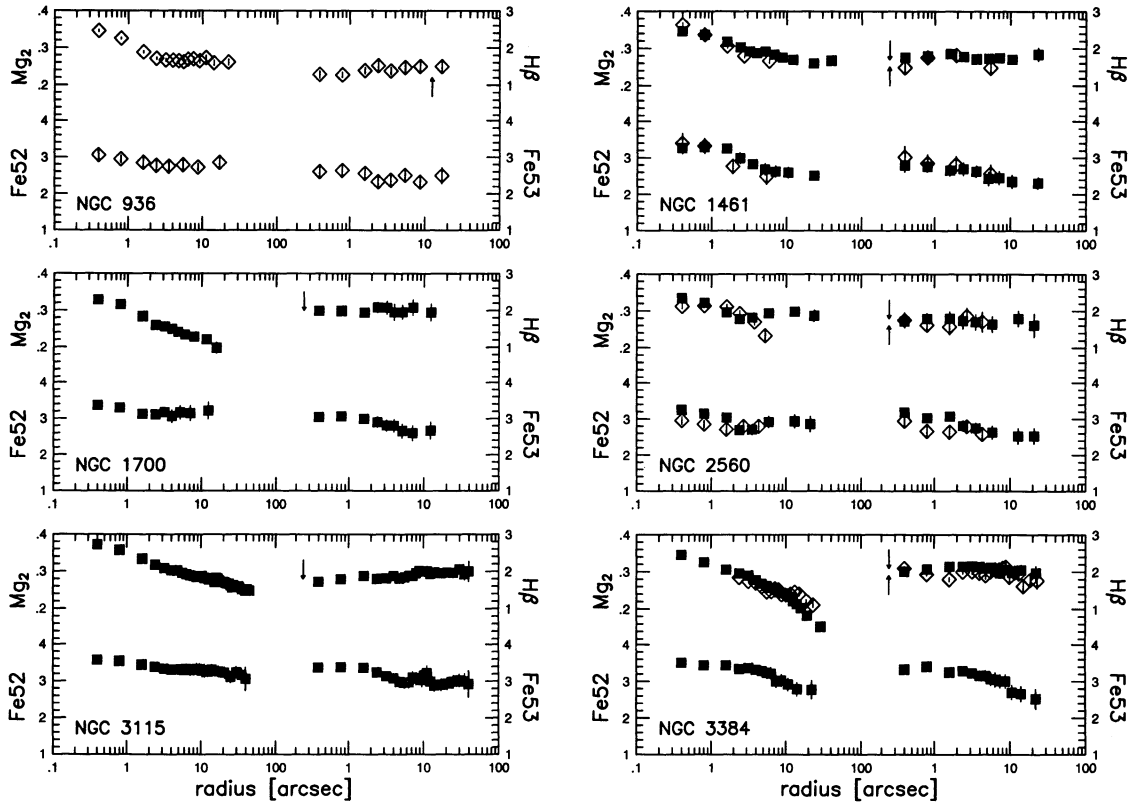

FIG. 10*a*

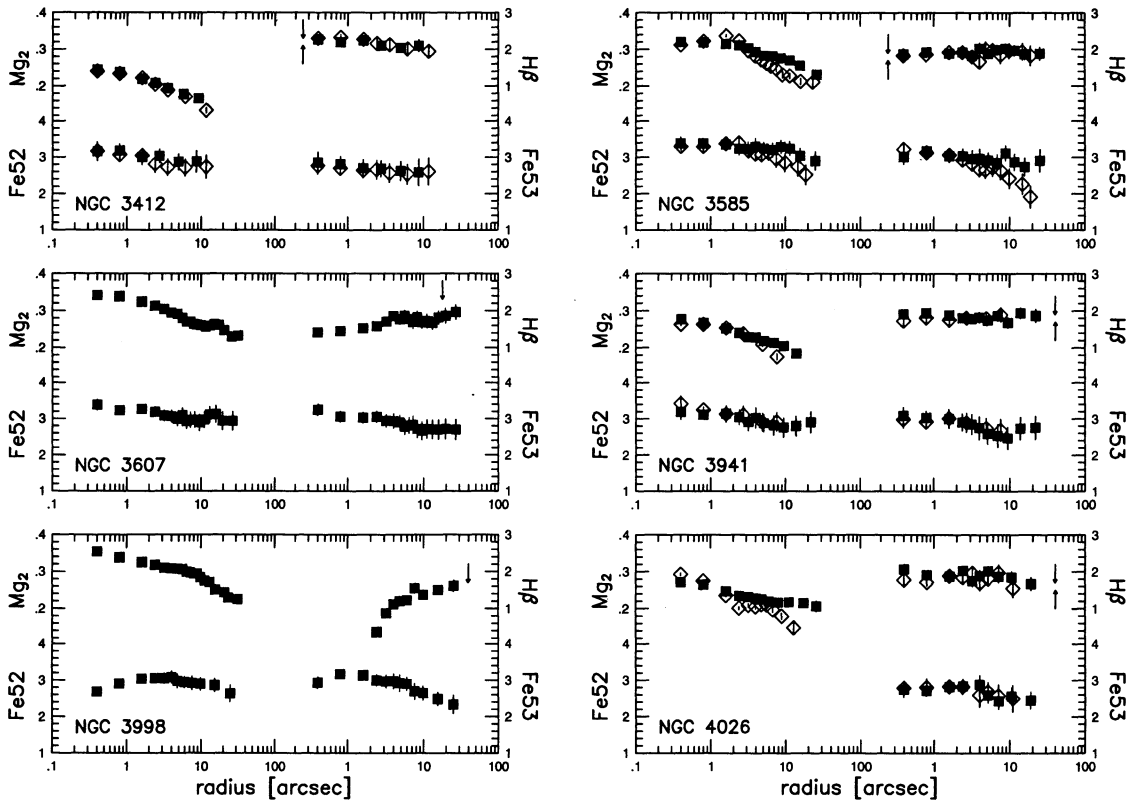

FIG. 10*b*

FIG. 10.—The Lick-IDS calibrated Mg_2, Hβ, Fe5270, and Fe5335 line strength results plotted for the full galaxy sample. Squares denote the major-axis measurements and diamonds represent minor-axis results (see Table 1 for position angles). Arrows are used in the Hβ panels to note the presence of contaminating emission in the Hβ feature. Downward-pointing arrows refer to the major-axis measurements and upward-pointing arrows refer to the minor-axis measurements. Points to the left of the arrows are contaminated by emission and points to the right are uncontaminated at the level of our measurements. For galaxies with no detectable emission at any radii, the arrows are placed at the far left of the panel. For galaxies whose Hβ index is contaminated by emission at all radii measured, the arrows are placed at the far right of the panel.

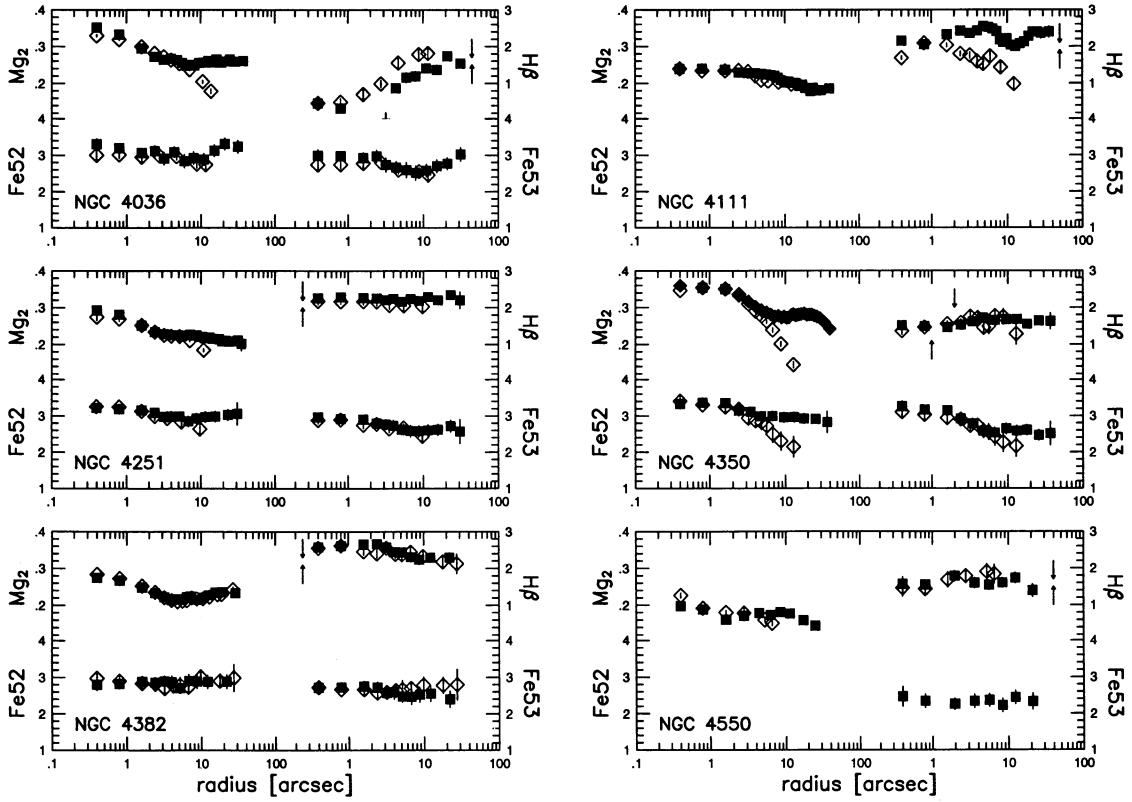

FIG. 10*c*

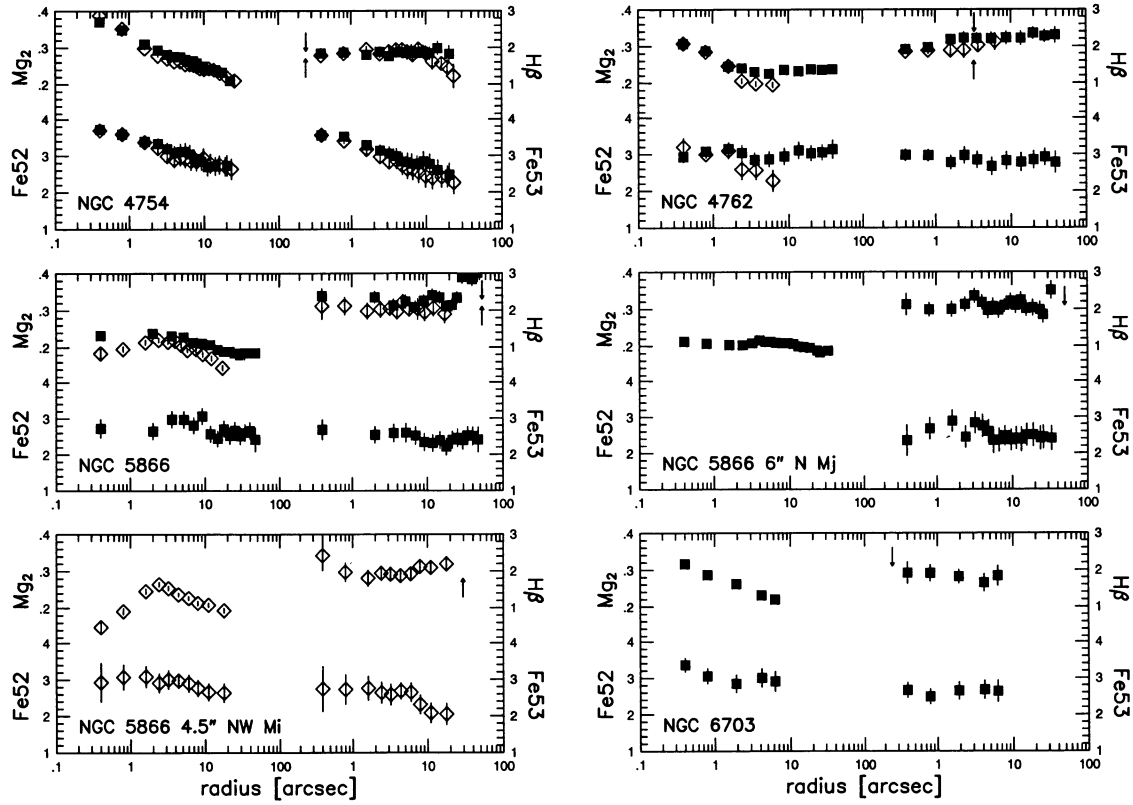

FIG. 10*d*

If the metal line strength gradients we measure are converted to metallicity gradients with the ages allowed to vary according to the Worthey prescription, the inferred metallicity gradients will be steeper than those given in § 4.3. The mean bulge gradient for all nine objects in the edge-on subsample is $\Delta[Fe/H]/\Delta\log r = -0.9$ if the Mg_2 index is used and a constant Hβ strength of 1.9 Å. This metallicity gradient is a factor of 1.6 larger than that inferred in § 4.3 for bulge Mg_2 gradients under the constant-age assumption. For this scenario the variation in the time since the last burst of star formation is $\Delta age/\Delta\log r \approx 7$ Gyr. If the MgFe or Fe4668 gradients are used, then the mean bulge gradient for the edge-on subsample is $\Delta[Fe/H]/\Delta\log r = -0.7 \pm 0.4$ with Hβ fixed to 1.9 Å and a variation in the time since the last burst of star formation of $\Delta age/\Delta\log r \approx 5$ Gyr. Note that Mg line strength gradients give larger metallicity and age gradients than either Fe or combination magnesium-iron gradients. The mean disk Mg_2 gradient for the subsample corresponds to a metallicity gradient of $\Delta[Fe/H]/\Delta(r/h) = -0.08 \pm 0.06$ or, when measured as a function of absolute physical size, $\Delta[Fe/H]/\Delta(r\ \mathrm{kpc}^{-1}) = -0.06$. In both cases the inferred age variations are $\Delta age/\Delta\log r < 1$ Gyr.

Only two of the objects in our sample show measurable Hβ gradients that are not caused by emission contamination. The first of these galaxies, NGC 4382, shows evidence for a young, less than 3 Gyr, central population on the basis of high central Hβ strength (2.57 Å). The Hβ profile in NGC 4382 shows a sharp decrease in strength with radius (see Figs. 9*c*, 9*d*, 10), indicating that the young population is limited in extent to the central regions. There are no signs of emission in the Hβ, [O III] 4959 Å, or [O III] 5007 Å lines, indicating that current star formation does not exist (at high levels). A remarkable feature of NGC 4382 is that for $r \gtrsim 4''$ the Mg and Fe line strengths *increase* with radius (see Fig. 10, Table 9). This is possibly because of the continuum from the young central population masking (filling in) the metal line strengths from the underlying old stars. Our CCD images confirm that the young population is limited to the central regions and that the color gradient in NGC 4382 in the range $4'' < r < 20''$ becomes *redder* with increasing radius (see Fig. 5). At larger radii the color profile of NGC 4382 displays the normal decrease in $B-R_C$ as typical of early-type galaxies. Similar color gradients for NGC 4382 were also shown by Bender & Möllenhoff (1987). Véron & Véron-Cetty (1985) measured the central $B-V$ color of NGC 4382 within a 15″.5 aperture to be 0.90 mag. We measure the blue ring to reach a maximum blue color of $B-R_C = 1.45$ mag at $r = 5''$. This is the only galaxy in our sample that displays such behavior and is a likely candidate for having experienced a late-time, possibly merger-induced (isophote twists are apparent) starburst (see e.g., Schweizer 1995).

The second galaxy with a measurable Hβ gradient is NGC 4754. This galaxy is the best example of real differences in the major- and minor-axis Hβ gradients. In NGC 4754 the major-axis profile is constant while the minor-axis Hβ values drop $\sim$0.8 Å below the major-axis values at the limit of our measurements (see Fig. 10). Since the metal line strength gradients in NGC 4754 are similar along both axes, the drop in Hβ could be interpreted as evidence for an age gradient along the minor axis that results in a older bulge population than in the disk. However, the presence of a bar in NGC 4754, aligned intermediate to the major and minor axis, complicates this interpretation.

The elliptical galaxy NGC 1700 contains a counterrotating component in the inner $\pm 3''$. As seen in Figure 10, where the line strength gradients for NGC 1700 are plotted logarithmically, the major-axis metallicity profiles decline smoothly, and no central enhancement is apparent in the region occupied by the counterrotating component. If the cause of these counterrotating components is the merging of low-luminosity disks or compact ellipticals, then one would expect that the central stellar populations should be metal-poor if the light in the inner regions were dominated by these accreted objects, as discussed by, e.g., Forbes, Franx, & Illingworth (1994). However, this and other studies (e.g., Franx & Illingworth 1988, 1990; Bender & Surma 1992) have not observed such a decrease in central metallicity in ellipticals with kinematically distinct nuclei. The Hβ profile for NGC 1700 is flat, exhibiting no significant change with radius over the full range of our measurements. No emission lines are found in our spectrum of NGC 1700, indicating that star formation is not likely to be currently occurring in the system. The smooth metallicity gradients and flat Hβ profile in NGC 1700 suggest that the kinematically distinct core has a stellar population similar to that of the underlying population in the galaxy's center.

The nearly edge-on SA0 NGC 5866 possesses an extensive dust lane along the major axis. Our major-axis Hβ profile suffers from emission contamination to the limit of our measurements. However, for $r \gtrsim 30''$, this contamination to the Hβ index is predicted to be low on the basis of the [O III] 5007 Å feature (see Table 9). The Hβ absorption in the disk of NGC 5866 at 1 scale length is the highest, Hβ = 2.89 Å, we measure in our total sample of objects at any radius. Since emission contamination would act to dilute the Hβ absorption, this high value is actually a lower limit.

5. DISUSSION

It is not clear if S0 galaxies have been more efficient at converting gas into stars than spiral galaxies or whether star formation in S0 galaxies dwindled to zero for lack of a replenishment mechanism. The number of processes that likely played a role in the formation of S0 galaxies is large and modeling is difficult, particulary of the gas physics. Thus, not only are the details of the mechanisms that govern the star-formation histories in S0 galaxies unknown, but, to a large extent, so are the identities of the key processes themselves. Recent studies of the structure and kinematics of bulges and disks have begun to address some of these outstanding issues, and preliminary results suggest that these processes are even more complex than initially believed (see Larson 1990).

The effect of environment on S0 galaxies has often been suggested as being a major player in their formation and evolution. In Table 8 we give some basic parameters of the groups or clusters in which the objects in our sample reside. Four of the S0 galaxies in our sample (NGC 2560, NGC 3115, NGC 3941, NGC 6703) are considered field galaxies. No significant differences were discovered between the line strengths of the S0 galaxies in our sample and these parameters. It has been suggested that the bluer colors of field elliptical galaxies could be due to small amounts of recent star formation (e.g., Lucey 1995). Of the four S0 galaxies in our sample that are in field environments, only NGC 3941 shows indications of recent star formation (Fisher 1994a).

As galaxy kinematic properties have been found to correlate with group/cluster velocity dispersion (see FIF),

TABLE 8

GROUP/CLUSTER PARAMETERS

Galaxy	Group/Cluster	Source	v_z (km s^{-1})	n	σ (km s^{-1})
NGC 936.....	...	N	1625	5	143
NGC 1461.....	...	G	1343	3	169
NGC 1700.....	...	G	3783	3	202
NGC 2560.....	...	RC3	5153	...	...
NGC 3115.....	...	F	1020	...	...
NGC 3384.....	M96 Group (Leo I)	N	969	7	98
NGC 3412.....	M96 Group (Leo I)	N	969	7	98
NGC 3585.....	...	G	1133	6	114
NGC 3607.....	Leo cloud	N	1703	7	92
NGC 3941.....	...	RC3	1185	...	...
NGC 3998.....	Ursa Major Cluster	N	1320	50	124
NGC 4026.....	Ursa Major Cluster	N	1320	50	124
NGC 4036.....	Ursa Major Cloud	N	1737	25	101
NGC 4111.....	Ursa Major Cluster	N	1320	50	124
NGC 4251.....	Coma I	N	830	21	204
NGC 4350.....	Virgo Cluster S	N	1497	113	664
NGC 4382.....	Virgo Cluster S	N	1497	113	664
NGC 4550.....	Virgo Cluster S	N	1497	113	664
NGC 4754.....	Virgo Cluster S	N	1497	113	664
NGC 4762.....	Virgo Cluster S	N	1497	113	664
NGC 5866.....	...	N	972	4	74
NGC 6703.....	...	F	1823	...	...

NOTES.—Sources of data: Nolthenius 1993 (N), Garcia 1993 (G), Faber et al. 1989 (F), and de Vaucouleurs et al. 1991 (RC3). Group/cluster names are given for objects residing in commonly known groups and clusters. Recession velocities (v_z) and group/cluster velocity dispersions (σ) are also given. For the objects that belong to groups and/or clusters, the recession velocities refer to the mean group/cluster velocity. Also shown is the number of members (n) assigned to the group/cluster.

correlations between line strength parameters and $\sigma_{\rm grp/cl}$ were investigated, but none found. According to models that rely on gas stripping by the cluster IGM, the differences between S0 galaxies in these different density regimes should be most apparent in their disks. The edge-on subsample of nine galaxies is not large enough for definitive trends to be explored, but the sample should increase, as it is now practical to obtain such data more readily. An additional complication is that the majority of the edge-on subsample has contaminating emission in its Hβ indices.

We find a number of important similarities between the behavior of S0 bulges and that of elliptical galaxies. Foremost is the general agreement between the S0 bulge central Mg_2-σ_0 relation and that found for elliptical galaxies. This agreement indicates that the bulges of S0 galaxies share some common evolutionary and star-formation mechanisms with elliptical galaxies. Similar structural parameters and fundamental plane correlations further reinforce the connection between these systems. However, the trend toward steeper Mg gradients in our S0 bulges and the larger amounts of rotational support typically found in S0 bulges (Kormendy & Illingworth 1982; Fisher 1994b) as compared to elliptical galaxies is evidence that differences exist.

Although it was once assumed that disk formation must have followed that of the bulge, this idea has been recently opened to question, and a number of formation mechanisms have been postulated that have bulges forming after the disk (see § 1). The results from the minor axes of the edge-on galaxies show that the bulges have metallicities in their outer parts that are significantly lower than those found in the disks. This suggests that the outer bulge stars were not once members of the disk and contradicts scenarios of heated disk material forming the bulge at late times. The similarity in the strength of the Hβ feature along the major and minor axes, and its constancy throughout the bulges and disks of the S0 galaxies, suggests that these components do not differ drastically in age. The models predict, however, that the nuclear regions are typically younger than the stars at larger radii in both the bulges and disks.

The Mg_2-σ_0 correlation for the S0 galaxy centers and the disk Mg_2-$v_{\rm circ}$ relation are powerful constraints on their formation histories. As spiral galaxies share qualitatively similar relations between luminosity and abundance, it is likely that mass is a main property governing the chemical history of disk galaxies (see, e.g., Tully, Mould, & Aaronson 1982). Concerning the metallicity gradients, a variety of mechanisms have been offered for setting up the radial abundance gradients in disks. Radial variations in IMF (e.g., Quirk & Tinsley 1973; Güsten & Mezger 1982), radial gas inflows (Tinsley & Larson 1978; Lacey & Fall 1985), and the effects of winds (see Larson 1990) are among the ideas that have been discussed. The trend toward the disks of earlier type galaxies having shallower abundance gradients suggests a link with Hubble type. As Hubble type correlates with mass (in the sense that earlier type disk galaxies are generally more massive than later types), the shallow metallicity gradients seen in our S0 disks could be understood in terms of more efficient star formation in galaxies with larger rotation speeds (see, e.g., Larson 1988).

Within the innermost regions, $r < 0.5$–$1\ r_e$, of the S0 galaxies in the edge-on subsample, the major- and minor-axis Hβ and metal line strength profiles are similar, and no differences along the separate axis are apparent. Beyond this bulge-dominated region the metal line strengths along the minor axis continue to decrease in comparison to the constant metal line strength profiles found throughout the S0

disks. The Hβ profiles along both the major and minor axes are, however, generally similar at all radii. This indicates that the outer parts of bulges are populated by stars that are older and metal-poorer than both the inner regions of the bulge and the disk stars at 1 h. These bulge stars, at $r > 1\ r_e$, are of low metallicity ([Fe/H] ≈ -0.7–0) compared with typical disk metallicities $\sim$0.25 dex higher in [Fe/H]. These observations are consistent with "outside-in" scenarios for the formation of bulges (see, e.g., Renzini 1995). In this picture the star formation begins first in the halo and progresses inward with inflowing, enriched gas building up the central metallicity and producing metallicity gradients (Larson 1975).

The time since the last major burst of star formation in the bulges and disks of S0 galaxies spans a wide range on the basis of the Worthey (1994) models. This range includes galaxies that are currently forming stars (NGC 5866), those that formed stars within the past few Gyr (NGC 4382), and those that seem to show no significant star formation within the last 8–10 Gyr. We stress that these ages do not refer to the galaxies as a whole but rather the time since the last burst of star formation. The fact that 50% of our S0 galaxies display emission lines (see Tables 2, 9) at some level indicates that low levels of star formation could be a common feature or at least that the ingredients for star formation are available. The strength of the Hβ feature is weighted by light and might often reflect only the most recent generation of stars and not the underlying substrate of a presumably older population. This range in time since the last episode of star formation is typical of that found for the nuclei of elliptical galaxies under the same assumptions about using Hβ as an age indicator (González 1993; FFI; Faber et al. 1995).

We emphasize that care should be taken in ascribing the central nucleus measurements as representative of the entire bulge component. Galaxy nuclei are their own, separate entities. The nucleus of a galaxy is the probable destination for dissipating gas, especially from transport to the nuclear region by a bar (see, e.g., Shlosman 1994) and will likely be the site of the most recent episode of star formation in early-type galaxies, so it is not surprising that our observations indicate that the youngest populations are generally found in the centers of the galaxies. Again, we caution that our line strengths measure the total integrated light from what is surely a mix of stellar populations. Spectra taken at slit positions other than the principal axes and offset from the nucleus would be valuable in determining a more complete picture of a galaxy's stellar content.

The combined effects of age and metallicity complicate straightforward interpretations of line strength measurements. It is clear that a number of steps could and should be taken to resolve some of the open issues here: (1) The difficulties encountered with the Hβ index when emission features are present needs to be addressed. Further blueward observations will be useful in obtaining measurements of the Hδ and Hγ features to check their consistency with the Hβ predictions and provide more complete age determinations (see, e.g., Jones & Worthey 1995). In particular, the need to clarify the source(s) of the Hβ feature is paramount. (2) The single-burst stellar-population models that we employ suffer from several limitations. The integrated starlight at any one point in a galaxy is likely a mixture of stars with differing abundance and age. Models with varying abundance ratios and multiple generations of star formation are a necessary progression in model development. (3) Pushing the measurements out to larger radii will be a useful step in examining the various predictions concerning galaxy formation.

6. CONCLUSIONS

In summary:

1. *Central metallicities.*—The increase of central Mg strength with velocity dispersion in S0 galaxies is similar to that seen in ellipticals. More observations of low-mass S0 galaxies would be useful to investigate whether the S0 galaxy Mg_2-σ_0 relation shows any deviations from the elliptical relation at low σ_0, as hinted by our data. The possibility that barred galaxies may systematically have Mg_2 strengths larger than predicted by the Mg_2-σ_0 relation suggests that additional gas inflow may have occurred in these systems.

The lack of a correlation between S0 galaxy Fe abundance and velocity dispersion—behavior that is also seen in elliptical galaxies—is an important point in understanding the star-formation histories of early-type galaxies. The absence of a trend with stellar velocity dispersion means that the net Fe production is largely decoupled from the traditional parameters that characterize galaxies, i.e., potential, mass (luminosity), and size.

2. Mg/Fe *ratios.*—The increase in S0 galaxy central Mg-to-Fe line-strength ratio with galaxy velocity dispersion, and therefore mass and size, is similar to that seen in elliptical galaxies. The centers of S0 galaxies share with ellipticals the behavior that the ratio of Mg to Fe is greater than the solar value for the luminous systems.

The results for the Mg/Fe ratios for the bulges (at 1 r_e) and disks (at 1 h) of our S0 galaxies are mixed. Some disks and bulges have Mg/Fe ratios larger than solar while others fall along the model tracks. However, a general property of the bulges and disks is that the level of Mg enhancement (with respect to Fe) decreases with galactocentric radius.

3. *Metallicity gradients.*—The Mg_2 differences observed along the major and minor axis of our edge-on galaxies are striking and point toward distinct bulge and disk star-formation histories. Although our disk line strength profiles typically extend to less than 2 scale lengths, broadband CCD images in B and R have been obtained that confirm that these shallow gradients extend to greater than 3 h. An exception to this behavior is observed in NGC 4350, in which we measure the disk Mg_2 strength to decline beyond 2 scale lengths.

Galaxy mass seems to be a primary parameter controlling the metallicity of the disks. The small disk gradients indicate that the formation of S0 disks, at least for radii $r \lesssim 2\ h$, was a process largely free from the processes that set up the radial variations in bulge abundance. The results from NGC 4350 are tantalizing, however, and suggest the possibility that steeper disk metal gradients may appear at larger radii. More data on the large-radius line strength behavior of edge-on S0 disks are needed to explore this possibility. Observations of the vertical chemical structure of disks would also be a useful tool for constraining their formation mechanisms.

4. *Ages.*—With the assumption that the Hβ feature can be used as an age indicator, a number of conclusions can be drawn from our data concerning S0 galaxy ages. Our line strength measures suggest that the nuclear regions contain a population of stars that is typically a few Gyr younger

than the bulk of the galaxy. The S0 galaxies span a range of Hβ strength that overlaps considerably with the range spanned by elliptical galaxies. However, S0 galaxies are not found with central Hβ strengths as low as those found in the most luminous ellipticals. A literal interpretation of the models suggests that the star-formation histories of S0 galaxies range from those containing significant amounts of recent activity (<1–3 Gyr) to those that seem to have been largely dormant for ~ 10 Gyr.

In conjunction with the bulge metal line strength gradients, the nearly constant Hβ profiles indicate that bulge age increases steadily with radius outward. This contrasts with the results found for the S0 disks in our edge-on subsample. Here, the shallow disk Mg_2 gradients, in conjunction with the nearly constant Hβ profiles, suggest that S0 disks have roughly constant age and metallicity to at least 1 scale length. Only in NGC 4350 is there evidence for the disk's having an older age at larger radius. In terms of relative ages, we find that the bulge and disk ages of S0 galaxies are not vastly different. The oldest stellar population in an S0 galaxy is found in the outer bulge and the youngest in the (bulge) center, with the disk having an age intermediate between the two.

We thank Reynier Peletier for a careful reading of the manuscript and an anonymous referee for many helpful suggestions. D. F. acknowledges partial support from HST grant GO.3551.01-91A.

This research has made use of the NASA/IPAC Extragalactic Database (NED), which is operated by the Jet Propulsion Laboratory, Caltech, under contract with the National Aeronautics and Space Administration.

APPENDIX A

NOTES ON INDIVIDUAL GALAXIES

A1. NGC 936

A prototypical barred galaxy, NGC 936 possess a prominent bar with P.A. = 77° (Kormendy 1983). Our minor-axis (P.A. = 45°) spectrum displays flat line strength profiles for $r \gtrsim 3''$. We detect [O III] 5007 Å emission, extending 10″ to either side of the nucleus along the minor axis.

A2. NGC 1461

NGC 1461 is a member of the edge-on subsample. To the limit of our observations, the major- and minor-axis profiles are similar.

A3. NGC 1700

The elliptical galaxy NGC 1700 possesses a counterrotating stellar core within the inner $\pm 3''$ along the major axis (González 1993). No emission features are seen in our major-axis spectrum, and the Hβ profile changes little with radius.

A4. NGC 2560

NGC 2560 galaxy is a member of the edge-on subsample. This galaxy is the faintest object in our sample ($B_T^0 = 14.08$), and further observations would be useful to push the measurements to larger radii and better constrain the line strength profiles.

A5. NGC 3115

NGC 3115 is a bulge-dominated S0 galaxy. Our major-axis surface brightness profile indicates that the bulge of NGC 3115 contributes more light than the disk for $r \gtrsim 5$ kpc. The major-axis Hβ profile of NGC 3115 displays a measurable rise in Hβ strength with radius (from 1.8 Å in the central regions to ~ 2.0 Å for $r \gtrsim 9''$). The color image of NGC 3115 (Fig. 5) displays a thin ($\lesssim 4''$) disk of constant color along the major axis surrounded by a bluer bulge region.

A6. NGC 3384

Our major- and minor-axis line strengths are dominated by light from the bulge component of NGC 3384, a barred S0.

A7. NGC 3412

Our major- and minor-axis line strengths for NGC 3412 are dominated by light from the bulge component of this barred S0. To the limit of our observations, the major- and minor-axis line-strength profiles are similar. The high central Hβ strength (2.26 Å) and declining Hβ gradients are suggestive of a younger central stellar population in comparison to the outer regions.

A8. NGC 3585

NGC 3585, an E/S0, contains noticably disky isophotes in the inner $\sim 20''$. Significant differences are found between the major- and minor-axis line strength profiles, similar to those found in the edge-on subsample. The color map of NGC 3585 (Fig. 5) displays a region of nearly constant color along the major axis while along the minor axis a blueing trend is seen. No emission features are present in the spectra, and the Hβ profiles are flat along both the major and minor axis.

A9. NGC 3607

NGC 3607 is inclined nearly face-on to the line of sight. Our major-axis Mg_2 profile displays measurable structure in the outer parts. A rapidly rotating gaseous disk is found along the major axis within the inner 15″.

A10. NGC 3941

NGC 3941 contains a prominent bar, misaligned $\sim 15''$ with respect to the major axis. An extended gaseous disk, counterrotating with respect to the stars, has been detected in [O III] 5007 Å (Fisher 1994a).

A11. NGC 3998

The nuclear regions of NGC 3998 have been classified as a low-ionization emission-line region (LINER) (Giuricin et al. 1991). Strong Hβ, [O III] 4959 Å, [O III] 5007 Å, and [N II] 5200 Å emission are apparent in our major-axis spectrum. Because of the strong emission, the line strengths in the central regions could not be reliably determined.

A12. NGC 4026

NGC 4026 is a member of the edge-on subsample. The minor-axis Mg_2 profile of this galaxy displays a plateau in Mg_2 strength between 2″ and 5″ before declining at larger radii. A similar feature is observed in the color map (Fig. 5). Extended [O III] 5007 Å emission is present throughout our major- and minor-axis data.

A13. NGC 4036

NGC 4036 is a member of the edge-on subsample. Dust is clearly present in our CCD images. Emission lines of Hβ, [O III] 4959 Å, and [O III] 5007 Å are present throughout our major- and minor-axis spectra. The major-axis Mg_2 profile of NGC 4036 is approximately constant, with radius for $r \gtrsim 10''$, in constrast to the minor-axis profile, which shows a smooth decline with radius. The apparent rise in Fe line strengths along the major axis is possibly an artifact of dust contamination.

A14. NGC 4111

NGC 4111 is a member of the edge-on subsample. This galaxy displays shallow Mg_2 profiles along both the major and minor axes with an enhancement only in the inner few arcseconds. The color map (Fig. 5) shows the presence of a compact red nucleus and central disk in this object. Extended [O III] 5007 Å emission is apparent along both the major and minor axes. Bad columns in our CCD detector prevented Fe5270 and Fe5335 indices from being derived.

A15. NGC 4251

NGC 4251 is a member of the edge-on subsample. The major-axis surface brightness profile of this galaxy displays complex structures in the form of multiple plateau/lens features, possibly resulting from a bar. The images suggest that the bulge of NGC 4251 dominates the light profile at large radii, though the complex light profile makes a disk/bulge decomposition difficult. The Hβ profiles in NGC 4251 show little change with radius.

A16. NGC 4350

NGC 4350 is a member of the edge-on subsample. The surface brightness profiles of this galaxy are well separable into $r^{1/4}$-law and exponential disk components. Following the region of constant Mg_2 strength with radius (for $10'' < r < 30''$), the major-axis Mg_2 profile shows an abrupt decline in strength with radius. The minor-axis Mg_2 gradient is the steepest in our entire galaxy sample. Weak [O III] 5007 Å emission is present in the inner regions ($r = \pm 5''$) of our major-axis spectrum. The line strength profiles along the major and minor axis of NGC 4350 differ dramatically and indicate a convincing separation into bulge and disk components (see Figs. 4, 5). Michard & Marchal (1993) described NGC 4350 as having a disk fully embedded in a spheroidal halo.

A17. NGC 4382

An ellipse-fitting algorithm applied to our R-band CCD image of NGC 4382 (M85) shows that the isophotes change position angle with radius (from P.A. = 60° in the nuclear regions to P.A. = 10° for $r > 100''$). The high central Hβ strength (2.57 Å) is suggestive of the presence of young stars in the inner regions. This conclusion is supported by the observation of a blue inner ring in the color image (Fig. 5). The lack of emission features in our spectra indicates that current star formation is likely not occuring.

A18. NGC 4550

NGC 4550 is a member of the edge-on subsample. Although this S0 contains two cospatial, counterrotating stellar disks (Rubin, Graham, & Kenney 1992; Rix et al. 1992), the line strength profiles appear unremarkable. The line strengths within the two disks are similar. Emission features throughout our spectra prevent an accurate determination of the stellar Hβ strength.

A19. NGC 4754

NGC 4754 contains a prominent bar, misaligned $\sim 40''$ with respect to the major axis. Although the major- and minor-axis Mg and Fe line strength profiles are similar, the minor-axis Hβ strength drops measurably for $r \gtrsim 15''$.

A20. NGC 4762

NGC 4762 is a member of the edge-on subsample. Beyond the bulge-dominated central regions, the major-axis line strengths in this galaxy show little change with radius to the limit of our measurements. We detect [O III] 5007 Å emission in the central $\pm 5''$ of our spectra.

A21. NGC 5866

Although significant structures are apparent in the metal line strength profiles of NGC 5866, an SA0, the extensive dust prevents reliable conclusions from being drawn about the behavior of the Mg and Fe indices. The minor-axis spectrum and minor-axis offset spectrum, which display a rise in Mg_2 strength with radius for $r \lesssim 3''$, suggest that either the dust or young stars are depressing the Mg_2 measurement in the disk. The high Hβ absorption strength found along the major axis at large radius (where emission contamination is small) is indicative of the presence of young stars.

A22. NGC 6703

NGC 6703 is a face-on field SA0.

APPENDIX B

INDIVIDUAL GALAXY FIGURES

Figure 10 plots the Lick-IDS–calibrated Mg_2, Hβ, Fe5270, and Fe5335 line strength results for the full galaxy sample. All line strengths are velocity dispersion–corrected and calibrated to the Lick-IDS system.

The full set of line strength results and measures of the [O III] 5007 Å emission line are given in Tables 9 and 10 (published in their entirety in computer-readable form in the AAS CD-ROM Series, Vol. 6). These tables are also available in electronic format from the authors.

TABLE 9

LINE-STRENGTH DATA

r	Fe4668	ϵ	Hβ	ϵ	Mg b	ϵ	Fe5270	ϵ	Fe5335	ϵ	[O III]	ϵ
NGC 936 P.A. = 45° Minor												
0.″4.....	6.34	0.18	1.28	0.10	4.39	0.11	3.06	0.14	2.60	0.15	0.27	0.07
0.8.....	6.04	0.14	1.27	0.07	4.30	0.08	2.94	0.11	2.64	0.12	0.27	0.05
1.6.....	5.63	0.16	1.39	0.09	4.23	0.09	2.85	0.12	2.56	0.14	0.18	0.07

NOTE.—Table 9 is published in its entirety in computer-readable form in the AAS CD-ROM Series, Vol. 6.

TABLE 10

Mg_2 DATA

r	Mg_2	ϵ
NGC 936 Minor		
0.″4.....	0.346	0.003
0.8.....	0.325	0.002
1.6.....	0.288	0.003

NOTE.—Table 10 is published in its entirety in computer-readable form in the AAS CD-ROM Series, Vol. 6.

REFERENCES

Abell, G. O. 1965, ARA&A, 3, 1
Balcells, M., & Peletier, R. F. 1994, AJ, 107, 135
Bender, R., Burstein, D., & Faber, S. M. 1993, ApJ, 411, 153 (BBF)
Bender, R., & Möllenhoff, C. 1987, A&A, 177, 71
Bender, R., & Paquet, A. 1995, in IAU Symp. 164, Stellar Populations, ed. P. C. van der Kruit & G. Gilmore (Dordrecht: Kluwer), 259
Bender, R., & Surma, P. 1992, A&A, 258, 250
Bender, R., et al. 1993, in Structure, Dynamics and Chemical Evolution of Elliptical Galaxies, ed. I. J. Danziger, W. W. Zeilinger, & K. Kjär (Garching: ESO), 3
Boroson, T. 1981, ApJS, 46, 177
Bothun, G. D., & Gregg, M. D. 1990, ApJ, 350, 73
Burstein, D. 1979a, Ph.D. thesis, Univ. California
———. 1979b, ApJ, 234, 435
Burstein, D., Faber, S. M., & González, J. J. 1986, AJ, 91, 1130
Caldwell, C. N. 1983, ApJ, 268, 90
Carlberg, R. G. 1984, ApJ, 286, 403
Carollo, C. M., & Danziger, I. J. 1994a MNRAS, 270, 523
———. 1994b, MNRAS, 270, 743
Carollo, C. M., Danziger, I. J., & Buson, L. 1993, MNRAS, 265, 553
Couture, J., & Hardy, E. 1988, AJ, 96, 867
Cowie, L. L., & Songaila, A. 1977, Nature, 226, 501
Davidge, T. J. 1992, AJ, 103, 1512
Davies, R. L., Burstein, D., Dressler, A., Faber, S. M., Lynden-Bell, D., Terlevich, R. J., & Wegner, G. 1987, ApJS, 64, 581
Davies, R. L., Sadler, E. M., & Peletier, R. F. 1993, MNRAS, 262, 650
de Vaucouleurs, G. H., de Vaucouleurs, A., Corwin, H. G., Buta, R. J., Paturel, G., & Fouqué, P. 1991, Third Reference Catalogue of Bright Galaxies (New York: Springer) (RC3)
Dressler, A. 1980, ApJ, 236, 351
———. 1984, ApJ, 281, 512
Dressler, A., Lynden-Bell, D., Burstein, D., Davies, R. L., Faber, S. M., Terlevich, R. J., & Wegner, G. 1987, ApJ, 313, 42
Faber, S. M. 1973, ApJ, 179, 423
Faber, S. M., Friel, E., Burstein, D., & Gaskell, C. M. 1985, ApJS, 57, 711
Faber, S. M., & Gallagher, J. S. 1976, ApJ, 204, 365
Faber, S. M., Trager, S. C., González, J. J., & Worthey, G. 1995, in IAU Symp. 164, Stellar Populations, ed. P. C. van der Kruit & G. Gilmore (Dordrecht: Kluwer), 249
Faber, S. M., Wegner, G., Burstein, D., Davies, R. L., Dressler, A., Lynden-Bell, D., & Terlevich, R. 1989, ApJS, 69, 763

Fisher, D. 1994a, in Mass-Transfer Induced Activity in Galaxies, ed. I Shlosman (Cambridge: Cambridge Univ. Press), 349
———. 1994b, Ph.D. thesis, Univ. California
Fisher, D., Franx, M., & Illingworth, G. 1995a, ApJ, 448, 119 (FFI)
Fisher, D., Illingworth, G., & Franx, M. 1995b, ApJ, 438, 539 (FIF)
———. 1995c, in IAU Symp. 164, Stellar Populations, ed. P. C. van der Kruit & G. Gilmore (Dordrecht: Kluwer), 453
Forbes, D. A., Franx, M., & Illingworth, G. D. 1994, ApJ, 428, L49
Franx, M., & Illingworth, G. D. 1988, ApJ, 327, L55
———. 1990, ApJ, 359, L41
Franx, M., Illingworth, G., & Heckman, T. 1989, ApJ, 344, 613
Garcia, A. M. 1993, A&AS, 100, 47
Garnett, D. R., & Shields, G. A. 1987, ApJ, 317, 82
Giuricin, G., Bertotti, G., Mardirossian, F., & Mezzetti, M. 1991, MNRAS, 250, 392
González, J. J. 1993, Ph.D. thesis, Univ. California
Gorgas, J., Efstathiou, G., & Aragón-Salamanca, A. 1990, MNRAS, 245, 217
Gorgas, J., Faber, S. M., Burstein, D., González, J. J., Courteau, S., & Prosser, C. 1993, ApJS, 86, 153
Gregg, M. D. 1989a, ApJS, 69, 217
———. 1989b, ApJ, 337, 45
Güsten, R., & Mezger, M. 1982, Vistas Astron., 26, 159
Gunn, J. E., & Gott, J. R. 1972, ApJ, 176, 1
Hubble, E. P. 1936, The Realm of the Nebulae (New Haven: Yale Univ. Press)
Hubble, E. P., & Humason, M. L. 1931, ApJ, 74, 43
Jones, L. A., & Worthey, G. 1995, ApJ, 446, L31
Kent, S. M. 1985, ApJS, 59, 115
Kormendy, J. 1977a, ApJ, 214, 359
———. 1977b, ApJ, 217, 406
———. 1979, ApJ, 227, 714
———. 1983, ApJ, 275, 529
———. 1993, in IAU Symp. 153, Galactic Bulges, ed. H. Dejonghe & H. J. Habing (Dordrecht: Kluwer), 387
Kormendy, J., & Illingworth, G. 1982, ApJ, 256, 460
Lacey, C. G., & Fall, S. M. 1985, ApJ, 290, 154
Larson, R. B. 1975, MNRAS, 173, 671
———. 1988, in Galactic and Extragalactic Star Formation, ed. R. E. Pudritz & M. Fish (NATO ASI Ser. C, 232) (Dordrecht: Kluwer), 459
———. 1990, PASP, 102, 709
Larson, R. B., Tinsley, B. M., & Caldwell, C. N. 1980, ApJ, 237, 692
Lauer, T. R., Stover, R. J., & Terndrup, D. 1983, The VISTA User's Guide (Lick Obs. Tech. Rep. 34) (Santa Cruz: Univ. California)
Lucey, J. R. 1995, in IAU Symp. 164, Stellar Populations, ed. P. C. van der Kruit & G. Gilmore (Dordrecht: Kluwer), 281
Maeder, A., 1992, A&A, 264, 105
Melnick, J., & Sargent, W. L. W. 1977, ApJ, 215, 401
Michard, R., & Marchal, J. 1993, A&AS, 98, 29
———. 1994, A&AS, 105, 481
Morgan, W. W. 1961, Proc. Natl. Acad. Sci., 47, 905
Nolthenius, R. 1993, ApJS, 85, 1
Oemler, A. 1974, ApJ, 194, 1
Oey, M. S., & Kennicutt, R. C., Jr. 1993, ApJ, 411, 137
Peletier, R. F., Davies, R. L., Illingworth, G. D., Davis, L., & Cawson, M. 1990, AJ, 100, 1091
Pfenniger, D. 1993, in IAU Symp. 153, Galactic Bulges, ed. H. Dejonghe & H. J. Habing (Dordrecht: Kluwer), 387
Quirk, W. J., & Tinsley, B. M. 1973, ApJ, 179, 69
Renzini, A. 1993, in IAU Symp. 153, Galactic Bulges, ed. H. Dejonghe & H. J. Habing (Dordrecht: Kluwer), 151
———. 1995, in IAU Symp. 164, Stellar Populations, ed. P. C. van der Kruit & G. Gilmore (Dordrecht: Kluwer), 325
Rix, H.-W., Franx, M., Fisher, D., & Illingworth, G. 1992, ApJ, 400, L5
Roberts, M. S., Hogg, D. E., Bregman, J. N., Forman, W. R., & Jones, C. 1991, ApJS, 75, 751
Rubin, V., Graham, J., & Kenney, J. 1992, ApJ, 394, L9
Sandage, A. 1961, Carnegie Inst. Washington Publ. 618
Sandage, A., & Tammann, G. A. 1981, Carnegie Inst. Washington Publ. 635 (RSA)
Sandage, A., & Visvanathan, N. 1978, ApJ, 225, 742
Schechter, P. L. 1990, in Dynamics and Interactions of Galaxies, ed. R. Wielen (Berlin: Springer), 508
Schweizer, F. 1995, in IAU Symp. 164, Stellar Populations, ed. P. C. van der Kruit & G. Gilmore (Dordrecht: Kluwer), 275
Schweizer, F., Seitzer, P., Faber, S. M., Burstein, D., Dalle Ore, C. M., & González, J. J. 1990, ApJ, 364, L33
Shlosmann, I. ed. 1994, Mass-Transfer Induced Activity in Galaxies (Cambridge: Cambridge Univ. Press)
Sil'chenko, O. K. 1993, AZh Pis'ma, 19, 701
Spitzer, L., & Baade, W. 1951, ApJ, 113, 413
Terlevich, R., Davies, R. L., Faber, S. M., & Burstein, D. 1981, MNRAS, 196, 381
Tinsley, B. M., & Larson, R. B. 1978, ApJ, 221, 554
Tully, R. B., Mould, J. R., & Aaronson, M. 1982, ApJ, 257, 527
Véron, P., & Véron-Cetty, M.-P. 1985, A&A, 145, 433
Vila-Costas, M. B., & Edmunds, M. G. 1992, MNRAS, 259, 121
Wakamatsu, K.-I., & Hamabe, M. 1984, ApJS, 56, 283
Weiss, A., Peletier, R. F., & Matteucci, F. 1995, A&A, 296, 73 (WPM)
Worthey, G. 1994, ApJS, 95, 107
Worthey, G., Faber, S. M., & González, J. J. 1992, ApJ, 398, 69 (WFG)
Worthey, G., Faber, S. M., González, J. J., & Burstein, D. 1994, ApJS, 94, 687
Zaritsky, D., Elston, R., & Hill, J. M. 1990, AJ, 99, 1108
Zaritsky, D., Kennicutt, R. C., Jr., & Huchra, J. P. 1994, ApJ, 420, 87 (ZKH)